(E81-10082) REMOTE ESTIMATION OF THE SURFACE CHARACTERISTICS AND ENERGY BALANCE OVER AN URBAN-RURAL AREA AND THE EFFECTS OF SURFACE HEAT FLUX ON PLUME SPREAD AND CONCENTRATION M.S. Thesis (Pennsylvania
N81-13435
G3/43
Unclas
00082

The Pennsylvania State University

The Graduate School

Department of Meteorology

Remote Estimation of the Surface Characteristics and Energy Balance Over an Urban-Rural Area and the Effects of Surface Heat Flux on Plume Spread and Concentration

Original photography may be purchased from
EROS Data Center
Sioux Falls, SD
57198

A Thesis in

Meteorology

by

Donald Charles DiCristofaro

Submitted in Partial Fulfillment
of the Requirements
for the Degree of

Master of Science

November 1980

I grant The Pennsylvania State University the nonexclusive right to use this work for the University's own purposes and to make single copies of the work available to the public on a not-for-profit basis if copies are not otherwise available.

Donald Charles DiCristofaro
Donald Charles DiCristofaro

The signatories below indicate that they have read and approved the thesis of Donald Charles DiCristofaro.

Date of Signature:	Signatories:
Sept 30, 1980	Toby R. Carlson, Associate Professor of Meteorology, Thesis Advisor
Sept. 30, 1980	Hans A. Panofsky, Evan Pugh Professor of Atmospheric Sciences
Oct. 6, 1980	Alfred K. Blackadar, Head of the Department of Meteorology

ABSTRACT

A one-dimensional boundary layer model is used in conjunction with satellite derived infrared surface temperatures to deduce values of moisture availability, thermal inertia, heat and evaporative fluxes. The Penn State satellite image display system, a sophisticated image display facility, is used to remotely sense these various parameters for three cases: St. Louis, MO; The Land Between the Lakes, KY; and Clarksville, TN.

The urban centers display the maximum daytime surface temperatures which correspond to the minimum values of moisture availability. The urban center of St. Louis and the bodies of water display the maximum nighttime surface temperatures which correspond to the maximum thermal inertia values. It is shown that moisture availability and thermal inertia are very much responsible for the formation of important temperature variations over the urban-rural complex.

Maximum heat flux and minimum evaporative heat flux values are found in the urban centers which correspond closely to the sites of maximum daytime temperatures. The opposite is found for the rural areas. Therefore, a large fraction of the variability in heat and evaporative fluxes is caused by variability in land use and in rates of evapotranspiration.

Satellite determined measurements of heat and evaporative fluxes and visible channel albedos are compared to corresponding values made by aircraft. In the case of surface heat flux the

PRECEDING PAGE BLANK NOT FILMED

agreement was poor; with surface evaporative flux there was some agreement; while the albedos agreed very closely.

The Willis and Deardorff method of estimating dispersion parameters is used to infer the effects of surface heat flux on the downwind plume spread and concentration of contaminants. The ground-level point concentrations are found to be largest for the smallest heat fluxes; however, the maximum ground-level point concentrations are found to be independent of heat flux. In view of the large variability of heat flux with land use, it is important to consider the land use in the downwind direction of a power plant.

TABLE OF CONTENTS

		Page
ABSTRACT		iii
LIST OF TABLES		vii
LIST OF FIGURES		viii
LIST OF SYMBOLS		xii
ACKNOWLEDGEMENTS		xiv
1.0	INTRODUCTION	1
	1.1 Statement of the Problem	1
	1.2 Purpose of the Thesis	2
2.0	THE PENN STATE SATELLITE IMAGE DATA MANIPULATION SYSTEM	5
	2.1 Past Method of Analysis	5
	2.2 Data Display and Analysis	6
	2.3 The Model	16
3.0	THE ST. LOUIS URBAN HEAT ISLAND	21
	3.1 Past Urban Heat Island Research	21
	3.2 Background August 23-24, 1978	24
	3.2.1 August 23 Daytime Temperatures	25
	3.2.2 August 24 Nighttime Temperatures	30
	3.2.3 August 23-24 Moisture Availability	32
	3.2.4 August 23-24 Thermal Inertia	34
	3.2.5 August 23 Surface Heat Flux	36
	3.2.6 August 23 Surface Evaporative Heat Flux	38
	3.3 Summary of Results	38
4.0	PROJECT STATE RESULTS	41
	4.1 Project STATE--The Tennessee Plume Study	41
	4.2 Background August 22-23, 1978	42
	4.3 The Land Between the Lakes August 22-23, 1978	47
	4.3.1 August 22 Daytime Temperatures	47
	4.3.2 August 23 Nighttime Temperatures	51
	4.3.3 August 22-23 Moisture Availability	51
	4.3.4 August 22-23 Thermal Inertia	54
	4.3.5 August 22 Surface Heat Flux	56
	4.3.6 August 22 Surface Evaporative Heat Flux	58
	4.4 Clarksville August 22-23, 1978	60
	4.4.1 August 22 Daytime Temperatures	60
	4.4.2 August 23 Nighttime Temperatures	60
	4.4.3 August 22-23 Moisture Availability	63
	4.4.4 August 22-23 Thermal Inertia	65
	4.4.5 August 22 Surface Heat Flux	67
	4.4.6 August 22 Surface Evaporative Heat Flux	67

TABLE OF CONTENTS (Continued)

		Page
	4.5 Cumberland Albedos	70
	4.6 Comparison of Aircraft Measurements with Satellite Derived Albedos, Surface Heat and Evaporative Fluxes	74
	4.7 Summary of Results	78
5.0	INFERRING THE EFFECTS OF SURFACE HEAT FLUX ON PLUME SPREAD AND CONCENTRATION OF CONTAMINANTS	80
	5.1 Atmospheric Dispersion Research	80
	5.2 Dispersion from an Elevated Point Source in the Convective Planetary Boundary Layer	82
	5.3 St. Louis and Cumberland Plume Characteristics	87
	5.4 Summary of Results	97
6.0	CONCLUSIONS	99
	APPENDIX - DESCRIPTION OF SIMPSON'S RULE	102
	REFERENCES	103

LIST OF TABLES

Table		Page
I	Initial Model Input Parameters for St. Louis	26
II	Initial Model Input Parameters for Land Between the Lakes and Clarksville	48
III	The Satellite Measured Albedos for 22 August 1978 vs. the Aircraft Measured Albedos for 17 August 1978 at Approximately 1400 LT	76
IV	The Satellite Measured Heat and Evaporative Fluxes for 22 August 1978 vs. the Aircraft Measurements for 27 August 1978	77
V	The Values Used to Compute w_* and X	89
VI	The Effect of Surface Heat Flux on Various Plume Spread and Concentration Parameters at a Distance of 1 km from the Source	90
VII	The Effect of Surface Heat Flux on Various Plume Spread and Concentration Parameters at a Distance of 2 km from the Source	91

LIST OF FIGURES

Figure		Page
1	The geographic locations of the three case studies: St. Louis, MO; The Land Between the Lakes, KY; and Clarksville, TN	3
2	Schematic representation of the Penn State satellite image data system	9
3	The 2048 by 2048 pixel image for 22 August 1978 at 1358 LST. The darkest areas indicate low temperatures and the lightest areas indicate high temperatures	11
4	The 512 by 512 pixel image chosen in Figure 3	11
5	The 128 by 128 pixel image chosen in Figure 4	14
6	The 128 by 128 pixel image chosen in Figure 4 with the cirrus cloud in the northeast portion of the image removed	14
7	Basic structure of the model	19
8	The 1200 GMT St. Louis soundings for 23 and 24 August 1978, along with the average of the two soundings	26
9	The base map used for the St. Louis case study along with the following key areas coded for easy reference . . . . . D Downtown St. Louis E East St. Louis P Forest Park H Horseshoe Lake G Granite City C Crop and Pasture Land	28
10	Daytime blackbody surface temperature analysis for 1330 LST on 23 August 1978 (°C)	29
11	Nighttime blackbody surface temperature analysis for 0230 LST on 24 August 1978 (°C)	31
12	Moisture availability analysis for 23-24 August 1978	33

LIST OF FIGURES (Continued)

Figure		Page
13	Thermal inertia analysis for 23-24 August 1978 (cal cm^{-2} K^{-1} $s^{-1/2}$)	35
14	Surface heat flux analysis for the early afternoon of 23 August 1978 (Wm^{-2})	37
15	Surface evaporative heat flux for the early afternoon of 23 August 1978 (Wm^{-2})	39
16	The base map used for the Land Between the Lakes case study along with the following key areas coded for easy reference	44
	LBL Land Between the Lakes	
	KL Kentucky Lake	
	JC Jonathan Creek	
	BR Blood River	
	LB Lake Barkley	
	LR Little River	
	DC Donaldson Creek	
	NSP Numerous Small Ponds	
	FCR Fort Campbell Restricted Area	
	F Forest and Brushwood	
	C Cropland and Pasture	
17	The base map used for the Clarksville case study along with the following key areas coded for easy reference	46
	CR Cumberland River	
	HP Hickory Point	
	WL Woodlawn	
	CB Corbandale	
	FCR Fort Campbell Restricted Area	
	NC Numerous Creeks	
	NSP Numerous Small Ponds	
	F Forest and Brushwood	
	C Cropland and Pasture	
18	The 1200 GMT Johnsonville, TN average sounding for 22 and 23 August 1978	48
19	The Land Between the Lakes daytime blackbody surface temperature analysis for 1400 LT on 22 August 1978 (°C)	49
20	The Land Between the Lakes nighttime blackbody surface temperature analysis for 0300 LT on 23 August 1978 (°C)	52

LIST OF FIGURES (Continued)

Figure		Page
21	The Land Between the Lakes moisture availability analysis for 22-23 August 1978	53
22	The Land Between the Lakes thermal inertia analysis for 22-23 August 1978 (cal cm^{-2} K^{-1} $s^{-1/2}$)	55
23	The Land Between the Lakes surface heat flux analysis for the early afternoon of 22 August 1978 (Wm^{-2})	57
24	The Land Between the Lakes surface evaporative heat flux analysis for the early afternoon of 22 August 1978 (Wm^{-2})	59
25	The Clarksville blackbody daytime surface temperature analysis for 1400 LT on 22 August 1978 (°C)	61
26	The Clarksville blackbody nighttime surface temperature analysis for 0300 LT on 23 August 1978 (°C)	62
27	The Clarksville moisture availability analysis for 22-23 August 1978	64
28	The Clarksville thermal inertia analysis for 22-23 August 1978 (cal cm^{-2} K^{-1} $s^{-1/2}$)	66
29	The Clarksville surface heat flux analysis for the early afternoon of 22 August 1978 (Wm^{-2})	68
30	The Clarksville surface evaporative heat flux for the early afternoon of 22 August 1978 (Wm^{-2})	69
31	The base map used for the Cumberland albedo study and the flight path for 17 August 1978 of The Pennsylvania State University's airplane, along with the following key areas coded for easy reference	72

LB Lake Barkley
KL Kentucky Lake
CR Cumberland River
CB Corbandale
WL Woodlawn
FCR Fort Campbell Restricted Area
NSP Numerous Small Ponds
NC Numerous Creeks
F Forest and Brushwood
C Cropland and Pasture

LIST OF FIGURES (Continued)

Figure		Page
32	The Cumberland surface albedo analysis (derived from visible satellite measurements) for 1400 LT on 22 August 1978 (%)	73
33	The nondimensional mean particle height ($\bar{Z}$) as a function of the nondimensional downwind distance from the source (X) (from Lamb, 1978)	85
34	The dimensionless overall standard deviations as a function of the dimensionless downwind distance from the source (from Willis and Deardorff, 1978) . .	85
35	The dimensionless mean cross-wind integrated concentration ($\overline{C^y}$) for an elevated source height of z_s=0.26h indicated by the vertical bar. The centerline of the plume is represented by the dashed line (from Lamb, 1978)	88
36	The ground-level values of the mean cross-wind integrated concentration ($\overline{C^y}(x,0)$) from a continuous point source of height z_s=0.26h as a function of the dimensionless downwind distance from the source (from Lamb, 1978)	88
37	The mean ground-level point concentration ($\bar{\chi}(x,0,0)$) as a function of the downstream distance from the source for H_o=200, 50, and 10 Wm^{-2}	95
38	The inverse heat flux $(H_o)^{-1}$ as a function of the distance from the source of maximum point concentration (x_{max})	96
39	Graphic representation of Simpson's Rule	102

LIST OF SYMBOLS

c	specific heat
$\bar{c}$	time dependent point mean concentration
c_p	specific heat at constant pressure
$\bar{C}^y$	dimensionless mean cross-wind integrated concentration
CIC	mean cross-wind integrated concentration
E_o	surface evaporative heat flux
$E_{o,pot}$	potential evaporation rate
F_d	downward terrestrial flux
F_u	upward terrestrial flux
$F(z)$	dispersion function for plume growth in the z direction
g	gravity
G_o	ground flux
$G(y)$	dispersion function for plume growth in the y direction
h	mixed layer height
H	effective source emission height
H_o	surface heat flux
k	von Karman constant
ℓ	length
L	Monin-Obukhov length
M	moisture availability
n	number of subintervals
P	thermal inertia
Q	source strength
R_n	net radiation
S	solar flux absorbed at the ground

LIST OF SYMBOLS (Continued)

t	time
t^*	dimensionless time
T	temperature
u_*	friction velocity
U	horizontal wind
w_*	convective velocity
x	distance from pollutant source
x_g	distance from the source of maximum ground-level cross-wind integrated concentration
X	dimensionless downwind distance from the source
Y	y coordinate nondimensionalized by h
z_a	height of the aircraft
z_s	stack height
$\overline{Z}$	non-dimensional mean particle height
λ	thermal conductivity
ρ	density
σ_v	turbulent lateral velocity
σ_w	turbulent vertical velocity
σ_y	cross-wind standard deviation of pollutant concentration
σ_z	vertical standard deviation of pollutant concentration
χ	ground-level concentration

ACKNOWLEDGEMENTS

I sincerely wish to thank Dr. Toby N. Carlson for the generous amount of guidance, time, and encouragement that he gave to me during the course of this research. Appreciation is extended to Dr. Hans A. Panofsky for his guidance and review of the manuscript. I am also grateful to James Cooper for his programming assistance which aided in the data analysis. Finally, a special note of thanks is due my parents for their constant encouragement.

This research was supported by the Environmental Protection Agency (EPA) under Contracts R-806048 and R-805640 and the National Aeronautics and Space Administration (NASA) under Contract NAS-5-24264. Computations were performed on an IBM 370/168 at the Computation Center and a PDP 11/10 at the Meteorology Department of The Pennsylvania State University.

1.0 INTRODUCTION

1.1 Statement of the Problem

In the past few years, many studies have been conducted to directly measure heat and evaporative fluxes, and substrate parameters, such as moisture availability and thermal inertia. Spittlehouse and Black (1979) used Bowen ratios and eddy correlation measurements to determine the evapotranspiration from forests. The major problem was that the vertical temperature and humidity gradients above the forest canopy were very small, generally less than $0.1°Cm^{-1}$ and $0.1\ gm^{-3}\ m^{-1}$, respectively. These small gradients were a result of the high degree of turbulent mixing generated by the large roughness of forests. Small errors in these measurements resulted in large errors in the determination of evapotranspiration. Other studies, including Hicks et al. (1975), also found it difficult to measure forest evapotranspiration.

On 26 April 1978, the National Aeronautics and Space Administration (NASA) launched a small Applications Explorer satellite as part of the Heat Capacity Mapping Mission (HCMM). The satellite carried a two-channel radiometer (0.5-1.1 μm and 10.5-12.5 μm) in a sun-synchronous orbit. The satellite had a resolution of .6 km and collected radiometric ground temperature data at approximately 0230 and 1330 LST which was close to the times of maximum and minimum surface temperatures. The satellite capabilities are discussed in detail by Price (1979). Dodd (1979), Kocin (1979), and Carlson et al. (1980) used data from the HCMM mission in conjunction with a one-

dimensional boundary layer model developed by Carlson and Boland (1978) to infer values for moisture availability, thermal inertia, heat and evaporative fluxes. The method used by these workers to determine such parameters from remotely sensed data required a considerable amount of time for processing the conventional batch computer data.

Once the problem of obtaining reliable surface heat flux data over a particular area has been solved, one application is to study the effect of a variable surface heat flux on plume spread and concentration. This can have a profound effect on the downwind spread and concentration of the plume.

1.2 Purpose of the Thesis

This research applies high-resolution surface temperatures obtained by the use of a sophisticated satellite image display system in conjunction with a one-dimensional boundary layer model to infer values of moisture availability, thermal inertia, heat and evaporative fluxes. The Penn State satellite image data manipulation system, discussed in detail in section 2.0, involves a faster, more reliable method for determining the surface and substrate parameters than that used in earlier HCMM efforts.

Three case studies, St. Louis, MO; The Land Between the Lakes, KY; and Clarksville, TN, are presented in sections 3.0 and 4.0. The geographic locations of these sites are displayed in Figure 1. The St. Louis case study was conducted for the purpose of investigating the surface energy balance and substrate parameters over a large urban

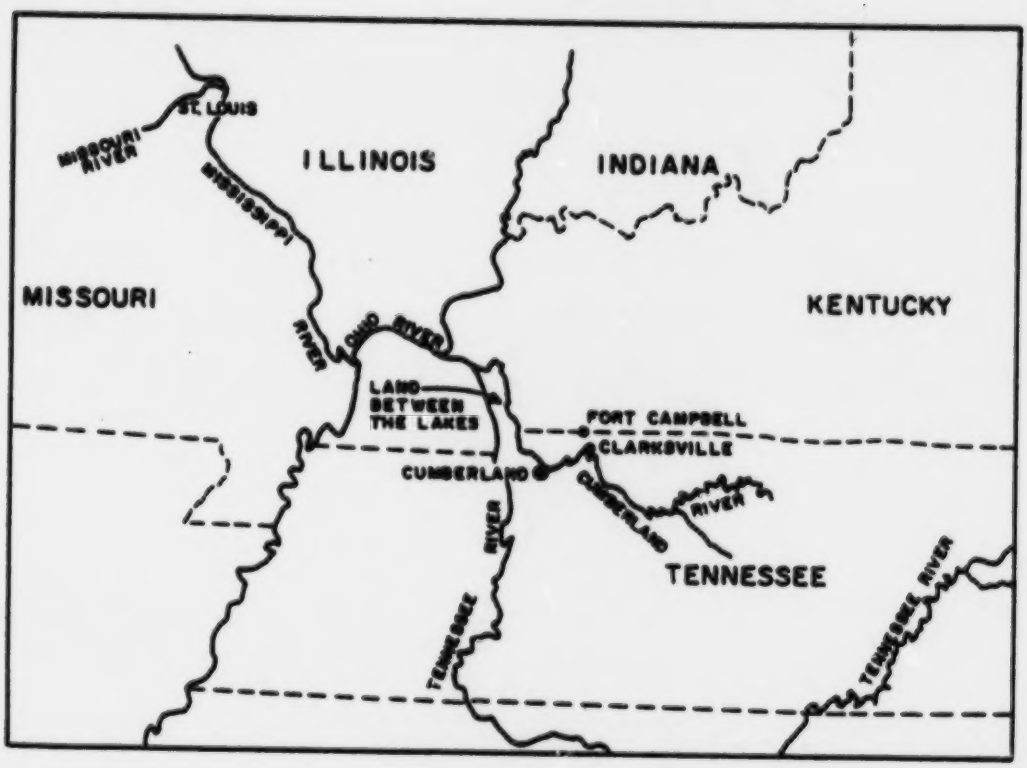

Figure 1. The geographic locations of the three case studies: St. Louis, MO; The Land Between the Lakes, KY; and Clarksville, TN.

area. The results are compared with past urban heat island research. The Land Between the Lakes and Clarksville case studies were conducted as a part of the Environmental Protection Agency's STATE, "Sulfur Transport and Transformation in the Environment", project. Albedo, heat and evaporative flux measurements obtained by aircraft are compared with the satellite measured values.

The surface heat flux values for the three case studies are examined to see how the surface heat flux varies over different terrain. The Willis and Deardorff method of estimating dispersion parameters is then used to study the effect of this variable surface heat flux on plume spread and concentration. Most importantly, the variation of the ground-level point concentrations with differing heat fluxes is examined. This is presented in section 5.0.

2.0 THE PENN STATE SATELLITE IMAGE DATA MANIPULATION SYSTEM

2.1 Past Method of Analysis

The sequence of computer programs used by Augustine (1978), Dodd (1979), and Kocin (1979) to extract the raw data from the computer tapes supplied by NASA and to grid the location of the working area has been superseded by a sophisticated image display system. This system, described in detail in section 2.2, saves a tremendous amount of time and increases the accuracy of the final product.

Augustine (1978) first used the program RECSTRA4 to extract a designated portion of a HCMM satellite picture from the raw data tape to a 512 by 512 area storage tape. The proper scan line and pixel from which the subset was to begin had to be specified by the user. This process was then repeated using the TGRFLOAS program to subset a 130 by 130 disk file from the 512 by 512 tape file. A histogram was also simultaneously produced. The histogram was used to assign characters equivalent to the digital data on disk. A character map was then produced which gave the user his first view of the area subsetted. If this area was not exactly what the user wanted, he would have to go through this time-consuming process again. Then the user would have to adjust the character assignments to obtain the best possible character map of the area desired. Identifiable physical features would have to be found from the character map to be used in conjunction with known reference points. This would involve the tedious process of counting the number of pixels in the X and Y direction from the character map.

A calibration equation for the HCMM data was used to convert the digital count or DN values (0-255) into temperatures (260-340°K). A water vapor correction suggested by Cogan and Willand (1974) was also applied to the calibration equation; however, the water vapor correction is now calculated through the program called NASRAD which is discussed in section 2.3.

The final analysis was then displayed through the use of a CALCOMP plotter to produce, for example, an isotherm analysis. The false-color-enhanced image created by a RAMTEK color display monitor was also used to display the final analysis.

This whole process has now been updated, so that the task of extracting, mapping, and contouring a desired area takes only one or two days as opposed to two or three weeks. The method of deriving the maps of moisture availability, thermal inertia, heat and evaporative fluxes is still used and this method is discussed in detail by Dodd (1979).

2.2 Data Display and Analysis

The purpose of the Penn State Satellite Image Data Display System is to enable the user to extract a workable area from a TIROS-N or HCMM satellite image and to transmit this area to an IBM 370 BAT (Batch and Terminal) file. A three step process is used to accomplish this. First, the data are stripped from the master data tape obtained from NASA and written to a scratch tape. HCMM data are written to the scratch tape as it appears on the master tape. TIROS-N data are calibrated and converted from thermal

energy units to absolute temperature, and are normalized on a scale of 0 to 255 where 0 is equal to -30°C and 255 is equal to 70°C. The scratch tape image is then displayed on a video monitor, and a smaller, workable area is selected for transmission. Finally, the data are transmitted to an active file on the IBM 370 via Penn State's RJE (Remote Job Entry) system.

The following equipment is used to extract and transmit an image to an IBM 370 BAT file:

1) PDP 11/10 minicomputer operating under RT-11 version 3.2

2) PDP 11/34 minicomputer operating under RSX-11M version 3.2

3) RK05 and RK07 disk drives

4) Digi data nine-track tape drive

5) Grinnell system (processor unit and T.V. monitor)

6) DR 11-B interface (direct measuring access) for the Grinnell processor

7) Grinnell monitor control box containing two 10-turn pots, one button, and one toggle switch

8) Modem (Dataphone 300/1200).

Once the master tape has been stripped, the communications file program called COMFIL is used to subset and transmit a workable area. A workable area usually encompasses approximately 4225 square kilometers. A series of commands are used to accomplish these tasks, and they are described below:

1) HELP -- Used to obtain a description of and instructions for running any of the following commands.

2) TAPE DISPLAY -- Displays the scratch tape image (or portion of it) on the Grinnell monitor.

3) GRAY SCALE -- Allows the user to adjust the resolution of the screen image.

4) COORDINATES -- Used to select a portion of the screen image to be enlarged or stored on disk.

5) READBACK -- Types the tape pixel coordinates and intensity of selected points on the video image.

6) SAVE TAPE -- Saves that portion of the tape image specified by the COORDINATES command.

7) HISTOGRAM -- Constructs a histogram of pixel intensities for the image file created by the SAVE TAPE or CLOUD command.

8) CLOUD -- Removes clouds from the image saved by the SAVE TAPE command.

9) DISK DISPLAY -- Displays on the T.V. monitor the disk file image created by the SAVE TAPE or CLOUD command.

10) CONVERT RJE -- Converts a disk file image into a form suitable for transmission to Penn State's RJE.

11) RECOVER -- Used to recover from RJE transmission errors.

A schematic representation of this analysis procedure is depicted in Figure 2. The image first displayed by the TAPE DISPLAY command is 2048 by 2048 pixels and an example of such an image is shown in Figure 3. This is a day infrared HCMM image for 22 August 1978 taken at 1358 LST. The area extends from Indiana and Ohio to Tennessee. The black areas indicate low temperatures; whereas, the white areas indicate high temperatures. The blackest regions in Figure 3 reveal cirrus clouds to the north and cumulus clouds to the south. The urban heat islands of Indianapolis, Indiana;

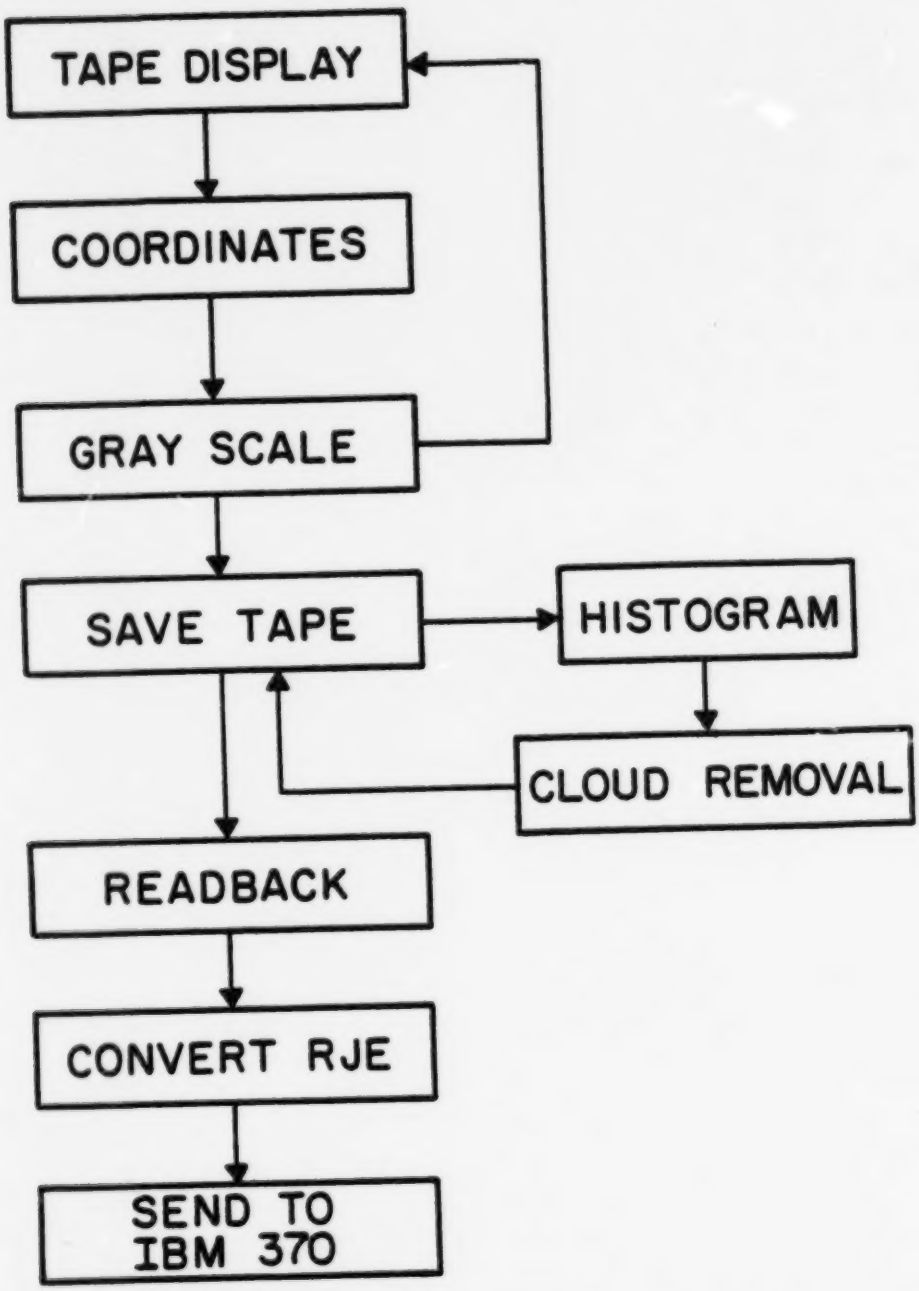

Figure 2. Schematic representation of the Penn State satellite image data system.

Figure 3. The 2048 by 2048 pixel image for 22 August 1978 at 1358 LST. The darkest areas indicate low temperatures and the lightest areas indicate high temperatures.

Figure 4. The 512 by 512 pixel image chosen in Figure 3.

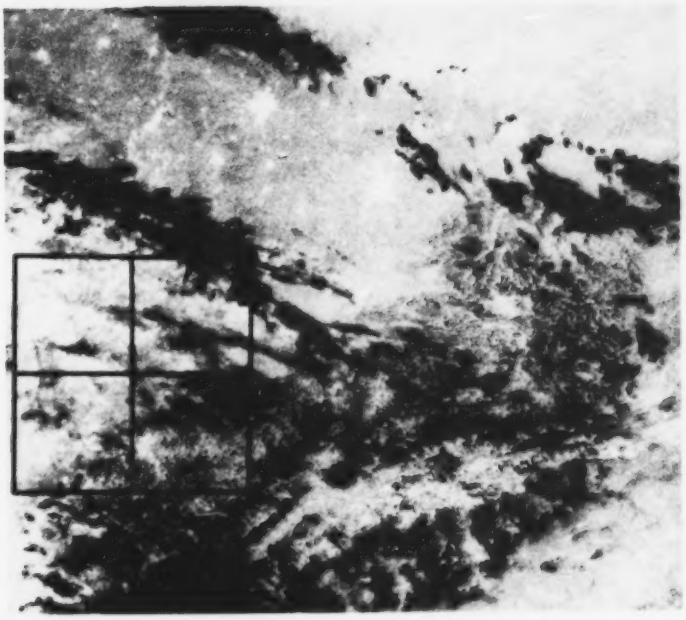

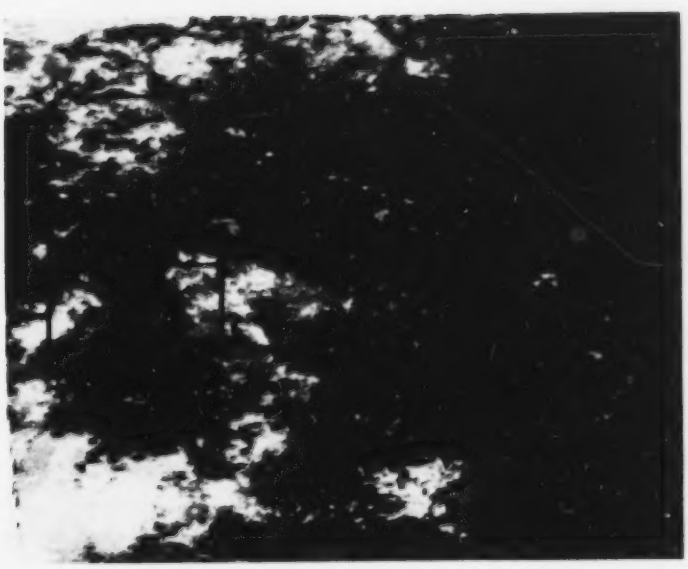

ORIGINAL PAGE IS
OF POOR QUALITY

Cincinnati, Dayton, and Columbus, Ohio are recognizable as the whitest areas in the northern portion of the image. The Land Between the Lakes, Kentucky, and Clarksville, Tennessee, the case studies described in section 4.0, are visible in the boxed area of the photo.

The COORDINATES program is used to extract the subsetted image. The height and width in pixels are specified and an appropriately scaled box containing crosshairs is superimposed onto the screen image. The crosshairs superimposed onto Figure 3 are 512 by 512 pixels. The box is moved by turning the X and Y knobs on the control box. TAPE DISPLAY is then used to display this smaller area. Figure 4 displays the area chosen to be enlarged in Figure 3. This same process is used again to choose the final, workable area. The box superimposed onto Figure 4 is 128 by 128 pixels and Figure 5 shows this final area. At any time, the GRAY SCALE command can be used to adjust the resolution of the screen image.

This image is now saved on disk by use of the SAVE TAPE command. HISTOGRAM is then used to construct a histogram of pixel intensities which provides information about the temperature distribution in the working area. Any abnormally cold spikes on the histogram indicate there are clouds in the final 128 by 128 area; therefore, it is necessary to use the CLOUD REMOVAL command. A thin cirrus cloud is visible in the upper right-hand corner of Figure 5. The low and high indices of the cloud, obtained from the histogram, along with a default value are entered with the CLOUD REMOVAL command. If the actual radius of a cloud is less than or equal to the specified value, the cloud will be patched over by the intensity values of the

Figure 5. The 128 by 128 pixel image chosen in Figure 4.

Figure 6. The 128 by 128 pixel image chosen in Figure 4 with the cirrus cloud in the northeast portion of the image removed.

ORIGINAL PAGE IS
OF POOR QUALITY

pixels on its periphery. If the cloud radius is larger than the supplied value, the cloud will be patched over by the default value, which is usually very black (intensity value 0) or very white (intensity value 255). This process is repeated until the cloud, such as the one in Figure 5, is removed. This cloudless image, which is shown in Figure 6, is then resaved on disk using the SAVE TAPE command.

The latitude and longitude (navigational coordinates) of the corner points are found via the READBACK command. READBACK types the tape pixel coordinates and intensity of selected points on the T.V. image. A set of crosshairs are displayed on the screen and they are positioned over prominent landmarks by turning the X and Y knobs on the control box. The tape coordinates with respect to the upper left-hand corner of the screen and the intensity of the pixel beneath the crosshairs are found by pushing the button on the control box. The READBACK reference points are matched with points of known latitude and longitude (reference points). The utility program called LONLAT, described by Augustine (1978), derives linear regression equations which describe the variation of latitude and longitude along the four borders of the 130 by 130 matrix. LONLAT then applies these equations to find the navigational coordinates of the corner points. The many inlets and peninsulas of the Land Between the Lakes are well represented, so the reference points are easily located and LONLAT is easily applied.

The 128 by 128 matrix is then converted into a form suitable for transmission by use of the CONVERT RJE command, and finally

transmitted to an active file on the IBM 370 via Penn State's RJE system. This file is transmitted as a 130 by 130 matrix to be compatible with LONLAT and other utility programs.

This whole process is then repeated for a night infrared image. The utility program called REGGIE, discussed in detail by Dodd (1979), is used to extract a region common to both the day and night working areas. REGGIE utilizes a calibration equation for the HCMM data which converts the DN values (0-255) into temperatures (260-340°K). Also included in this calibration equation is a water vapor correction that is calculated through the program called NASRAD. NASRAD computes the temperature difference between the observed ground surface temperature and the temperature measured by the radiometer in the 11 μ atmospheric window. The attenuation of energy is computed by applying the radiative transfer equation to an atmosphere consisting of layers for which the average temperature, pressure, and humidity are specified.

Before the final analysis can be made, the output from REGGIE must be coupled with output from the model which produces temperature as a function of moisture availability and thermal inertia. The model is discussed briefly in section 2.3.

2.3 The Model

Boland (1977), Dodd (1979), Kocin (1979), and Carlson et al. (1980) have thoroughly documented Carlson and Boland's technique of inferring moisture availability, thermal inertia, heat and evaporative fluxes. This method is briefly discussed below.

The one-dimensional boundary layer model was developed to investigate the importance of various terrain and atmospheric variables on the surface temperature and heat flux. Monin-Obukhov theory is used with an implicit K-type parameterization for the eddy fluxes in the surface layer. Net Radiation (R_n) is the primary forcing with no advection or anthropogenic heat sources included:

$$R_n = H_o + E_o + G_o \quad . \tag{1}$$

The surface heat flux (H_o) is expressed as a function of an eddy and molecular diffusivity, and a vertical potential temperature gradient. The water vapor flux (E_o) is expressed as a function of an eddy and molecular diffusivity for water vapor, and a vertical mixing ratio gradient. The ground flux (G_o) is parameterized in terms of the soil thermal conductivity and the temperature gradient immediately below the soil-air interface.

The net radiation is calculated from the radiative fluxes at the surface by:

$$R_n = S + F_d - F_u \quad , \tag{2}$$

where S is the solar flux absorbed at the ground, F_d is the downward terrestrial flux, and F_u is the upward terrestrial flux. Augustine (1978) gives a detailed explanation of the radiative transfer model.

The basic structure of the model which includes a substrate layer, transition layer, surface layer, and mixing layer is depicted

in Figure 7. Input parameters for the model include the temperature of the lowest level in the ground ($\sim$ 1.5 m), roughness length, albedo, surface wind speed and direction, precipitable water, ground emissivity, and turbidity of the atmosphere. A sounding of the atmospheric temperature and dewpoint extending from the surface to approximately 600 mb is an important input parameter. An average sounding of the day desired and the day before is used as initial conditions.

The mixed layer height (h) is calculated through a formulation developed by Tennekes (1973) in which h grows throughout the day as a consequence of the surface heat flux (H_o) from below and entrainment of air with a higher potential temperature from above. The heat flux becomes dependent on the temperature lapse rate near the ground at night when the upward heat flux disappears. The model then uses a method developed by Blackadar (1979) where the nighttime turbulence is calculated as a function of the Bulk Richardson Number in the surface layer. This formulation is used to simulate the boundary layer at night during which turbulent episodes occur.

The model is initialized at 0600 LST and allowed to proceed for a day. The model is reinitialized, after each cycle, with incremented values of moisture availability (.05 - 1.0) and thermal inertia (.005 - 0.1) until sixteen cycles are completed.

Moisture availability (M) is the fraction of maximum possible evapotranspiration for a saturated surface. Tanner and Pelton (1960) define M as

$$M = \frac{E_o}{E_{o,pot}} \qquad (3)$$

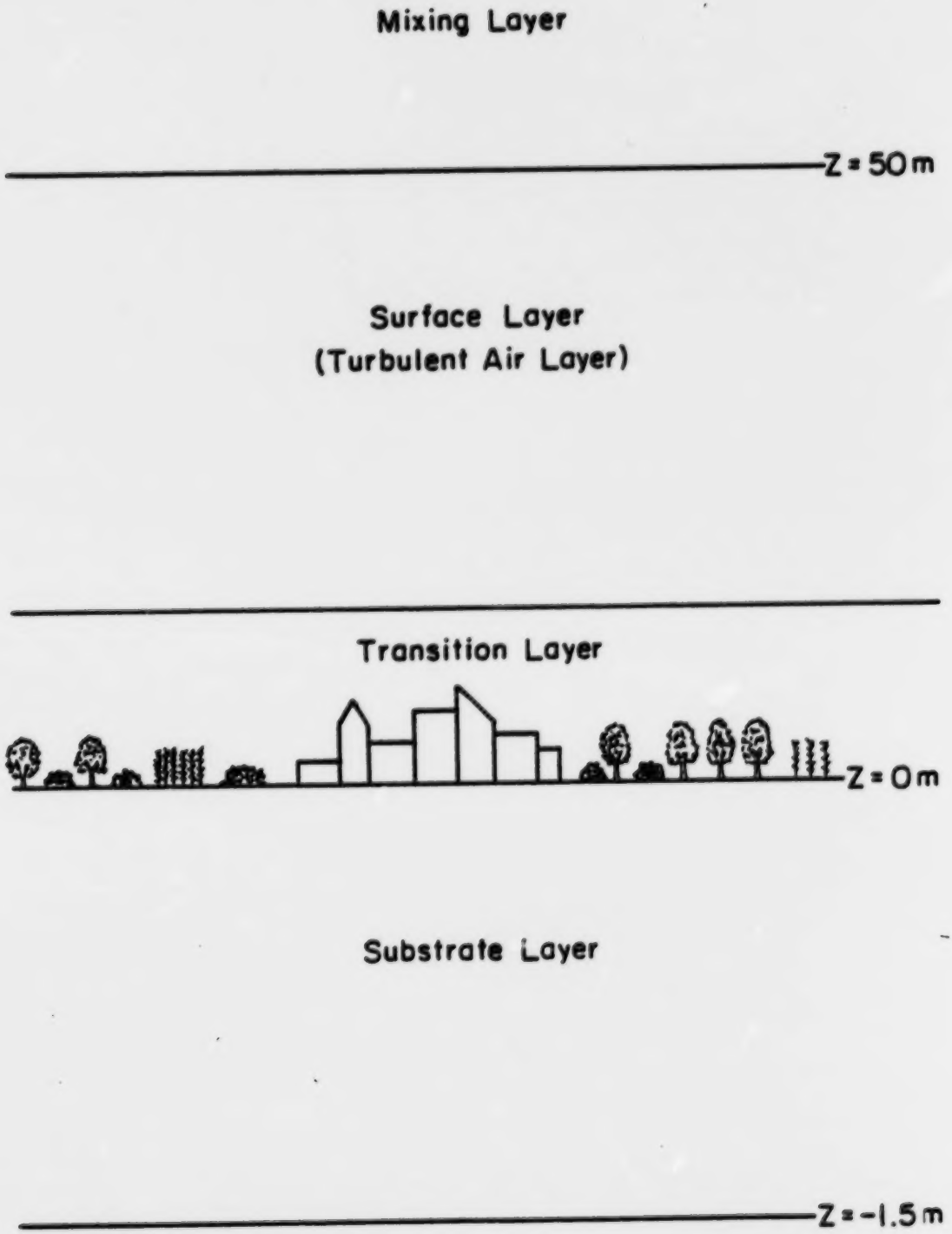

Figure 7. Basic structure of the model.

where E_o is the surface evaporation rate and $E_{o,pot}$ is the potential evaporation rate or the rate of evaporation from a saturated surface at temperature T_o. Moisture availability takes into account the reduction in the evaporation efficiency due to subsaturation of the surface air. The range of M is near zero for completely dry surfaces to 1.0 for saturated terrain. M is initialized in the model and held constant throughout the day. This is in agreement with Nappo (1975) who found that the specification of a diurnal range for M offers little advantage in modeling the surface fluxes.

Idso et al. (1976) maintain that internal and external factors must be taken into account when one looks at the diurnal surface temperature variation of any substrate material. Thermal conductivity (λ), density (ρ), and specific heat (c) of the substrate are internal factors which are used to define thermal inertia (P):

$$P = (\lambda \rho c)^{1/2} \tag{4}$$

which has the units of cal cm^{-2} K^{-1} $s^{-1/2}$ or Wm^{-2} K^{-1} $s^{1/2}$. The latter units are called thermal inertia units (TIU) where approximately 400 TIU are equivalent to .01 cal cm^{-2} K^{-1} $s^{-1/2}$. Solar radiation, air temperature, atmospheric precipitable water content, wind, etc. are some of the external parameters which affect the amplitude of the diurnal surface temperature wave.

As will be shown, the thermal inertia is most responsible for shaping the nighttime temperature pattern; whereas, the moisture availability has a greater effect on the temperatures during the day.

3.0 THE ST. LOUIS URBAN HEAT ISLAND

3.1 Past Urban Heat Island Research

Man has altered his environment in many ways with urbanization and industrialization being the best examples. The fact that urban areas are warmer than their rural surroundings has been known for a very long time. Luke Howard first published evidence of the urban heat island in 1833 when he showed that air temperatures measured in London were about 1.1°C higher than those in outlying areas. In 1927, Wilhelm Schmidt was the first to use an automobile to obtain a temperature analysis of a city. Since then, many studies have been conducted to determine the climatic impact of altering the terrain.

There are many reasons why cities possess a different climate than their environs. Landsberg (1979) maintains that the radical change in surface characteristics is most important in creating the heat island. Cities are made up mostly of brick, concrete, and asphalt which are believed to have a high heat conductivity and capacity. The heat stored during the day is slowly released at night causing warmer surface temperatures in the city. The anthropogenic heat produced from combustion (space heating, manufacture, transportation, lighting) can contribute 15 to 30% of the total heat budget. In fact, in Manhattan this heat source can contribute two and a half times the solar input in the winter. The tall buildings of the city increase the chance of multiple reflections of radiation. There is also a reduction in albedo, evaporative heat flux, and ventilation.

Duckworth and Sandberg (1954) studied three California cities of various sizes. The temperature was found to increase from rural to urban centers in direct proportion to the structure density of the city. Chandler (1965) conducted a 30 year study of the climate of London. He found that the city had more days with exceptionally high temperatures and fewer with low temperatures compared to the rural surroundings.

Mitchell (1961) gives three reasons why urban heat islands are not topoclimatic anomalies that would exist even in the absence of a city. First, cities of completely different topography possess heat islands. Second, the heat island is comparatively weaker on Sundays when industry and other urban activities are at a minimum. Third, Mitchell found that the intensity of the urban heat island increases with increased size and population of a city.

In 1971, an extensive five-year investigation called METROMEX was undertaken to see how St. Louis affects summer weather. White et al. (1978) found an extreme difference of 15°K in maximum infrared surface temperatures between industrial and undeveloped land. Solar noontime albedo values were found to vary from 15-17% for rural land in contrast to 12-13% for urban land. Measurements showed that the energy loss by emitted radiation is inversely related to the amount of vegetation in the St. Louis area during mid-August. Changnon (1978) found that within 40 km of the city in the summer, increases in the frequency of occurrence of various thunderstorm characteristics ($\sim$ +10 to 115%), hailstorms (+3 to +330%), various heavy rainfall characteristics (+35 to +100%), and strong gusts (+90 to +100%) occurred.

Braham and Wilson (1978) found from radar echo measurements that St. Louis exerts a substantial influence on the heights of convective clouds. There is roughly a twofold probability of finding the tallest echo over and downwind of the city in the summer during the midday and late evening hours.

It has only been during the last six years that satellite radiation data have been used to study the urban heat island. Carlson et al. (1977) used data from the NOAA-3 VHRR (Very High Resolution Radiometer) to study the infrared radiative (blackbody) surface temperature distribution for the Los Angeles area. The highest morning temperatures were found over the industrial zone, and in the evening the highest temperatures occurred over the central business district and residential areas. Matson et al. (1978) used the NOAA-5 satellite to detect more than fifty urban heat islands in the mid-western and northeastern United States on a cloud-free summer evening. The maximum urban-rural temperature differences ranged from 2.6°C to 6.5°C. Carlson et al. (1980) used HCMM infrared satellite temperature measurements in conjunction with a one-dimensional boundary layer model to infer the distribution of surface heat and evaporative fluxes, ground moisture availability, and thermal inertia. A reduction of evaporation and moisture availability along with an increase of sensible heat flux was found over urbanized areas and over cropped areas with low vegetative cover. The thermal inertia distribution was ill-defined and its variation between urban and rural areas was quite small.

This has been a very brief review of past urban heat island research. A detailed review of recent urban climatology studies is given by Oke (1979a).

3.2 Background August 23-24, 1978

St. Louis, the largest city of Missouri, is situated on the west bank of the Mississippi River approximately 16 km south of its junction with the Missouri River. St. Louis is one of the chief cities and major industrial centers of the midwest. The city has a population of approximately 623,000 making it the eighteenth largest city in the United States. The city is spread along 31 km of the Mississippi River and rises gently to the west to an elevation of 142 meters. St. Louis county, which extends all along the city's western perimeter, has more rolling terrain. Except for industrial parks, most of St. Louis county is residential, with the western portions being somewhat rural. The other counties are more rural and forested. In contrast, most of the St. Louis metropolitan area on the Illinois side of the Mississippi River is industrial. The urban areas there are partly flood plain; however, there are bluffs in some areas. The largest urban center on the eastern bank of the Mississippi River is East St. Louis which has a population of approximately 70,000.

The weather in St. Louis on 23-24 August 1978 was dominated by a large ridge of high pressure centered over West Virginia. Clear skies and temperatures around 35°C and nighttime temperatures around 18°C were recorded at the airport. Precipitation had not occurred

over the St. Louis area for at least a week; therefore, the ground can be expected to have been quite dry.

The satellite images were taken twelve hours apart on 23 August 1978 at approximately 0230 LST and 1330 LST. The model output was for 1330 LST on 23 August and 0230 LST on 24 August; thus, it was assumed that the nighttime satellite image occurred 24 hours after its satellite orbit time. It is believed that this reversal of orbit times did not affect substantially the final results. Carlson et al. (1980) assumed stationarity in the temperature response between two days as a basis for reversing the order of the day/night sequence in the model.

Some of the initial parameters used for the St. Louis model run are listed in Table I. The 1200 GMT soundings for 23 and 24 August 1978 are shown in Figure 8. The average of these two soundings, also seen in Figure 8, was used as input to the boundary layer model. The base map along with key areas that have been coded for easy reference is displayed in Figure 9.

3.2.1 August 23 Daytime Temperatures

The daytime surface blackbody temperatures displayed in Figure 10 show a wide spread of values ranging from 45°C to 29°C. As expected, the urban areas show the highest temperatures. Surface temperatures greater than 43°C are recorded in downtown St. Louis (D) with two maxima of 45°C centered along the interstate highway. Granite City (G), a highly industrialized area, exhibits a maximum of 45°C and an area of 45°C is also centered over the urbanized area just south of Jennings.

Table I. Initial Model Input Parameters for St. Louis

Ground Temperature at the Base of the Layer	290°K
Roughness Length	25 cm
Precipitable Water	2.54 cm
Albedo	.19
Emissivity	1.0
Wind Speed at $z \sim 3$ m	3.6 $msec^{-1}$
Direction	210°

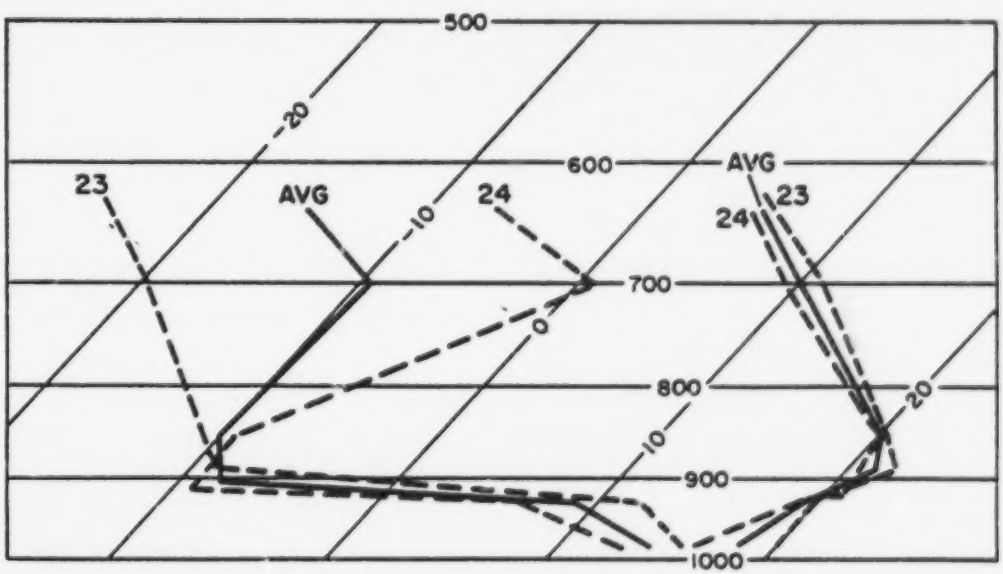

Figure 8. The 1200 GMT St. Louis soundings for 23 and 24 August 1978, along with the average of the two soundings.

Figure 9. The base map used for the St. Louis case study along with the following key areas coded for easy reference:

D Downtown St. Louis

E East St. Louis

P Forest Park

H Horseshoe Lake

G Granite City

C Crop and Pasture Land

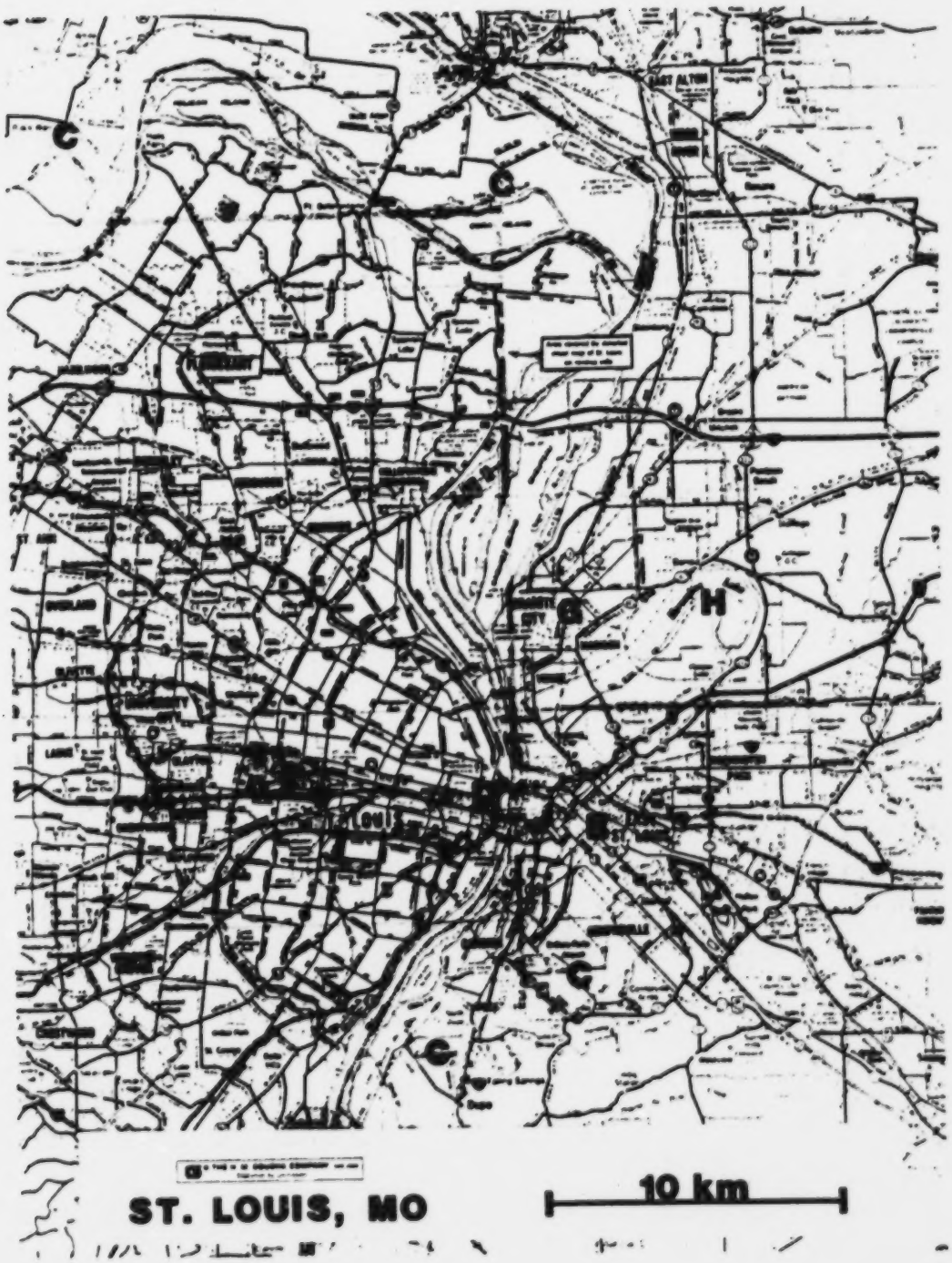

ORIGINAL PAGE IS
OF POOR QUALITY

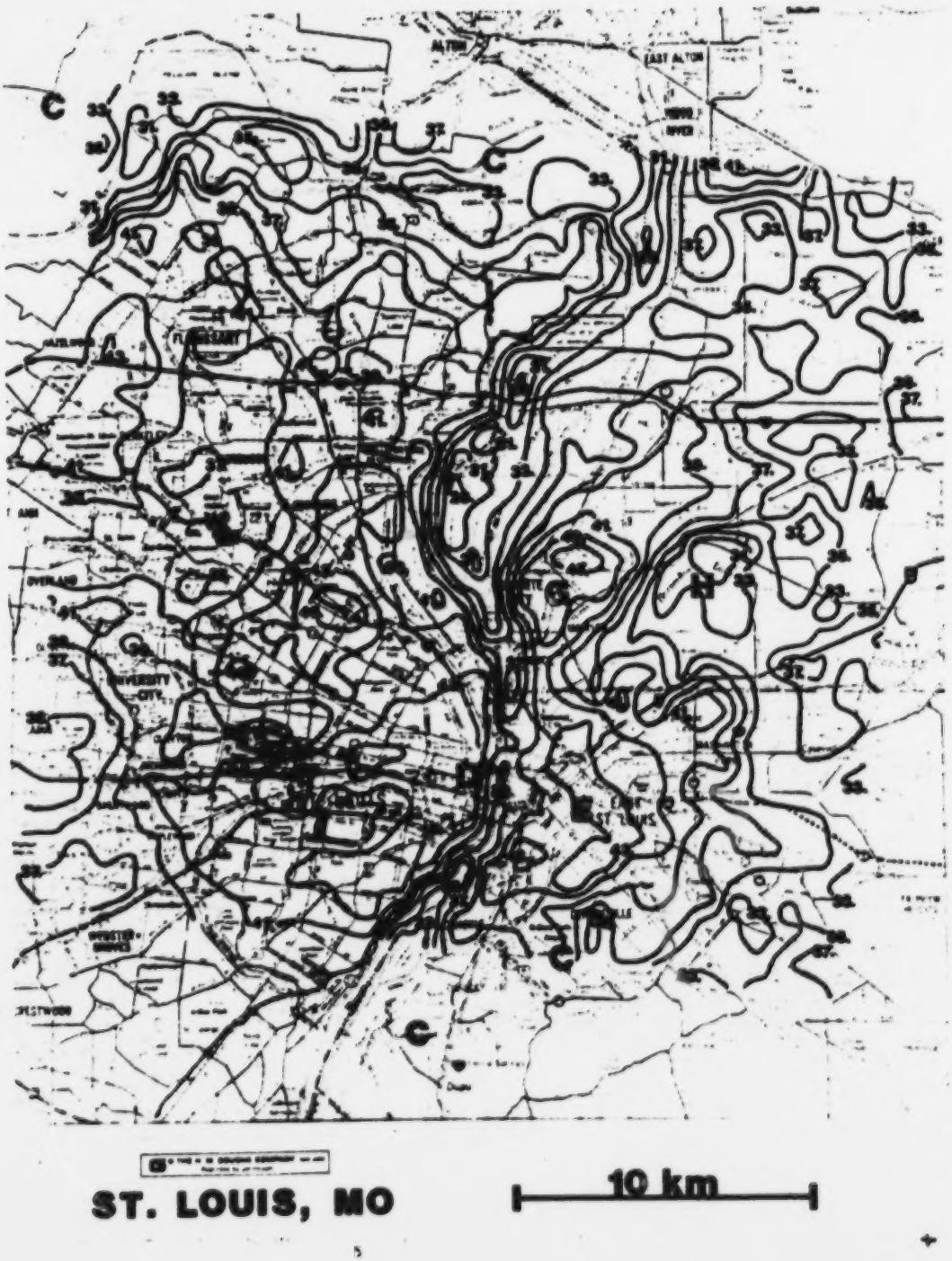

Figure 10. Daytime blackbody surface temperature analysis for 1330 LST on 23 August 1978 (°C).

The highly industrialized and urbanized area of East St. Louis (E) shows a temperature maximum of 43°C. An area of 41°C is also seen just south of Horseshoe Lake over Fairmont City, an industrial and residential area.

The physical and thermal properties of the city, along with the heat derived from industrial space heating, contribute to the high temperatures. Areas of maximum temperature outside the urban complex may be associated with industrial parks. Nkemdirim (1976) maintains that these high temperatures are partly due to the enhanced transfer of heat into the atmosphere through chimneys, the lower aggregate specific heat of the industrial park fabric, heavy truck traffic, and the enhanced horizontal mixing of air currents due to low density developments.

A 6°C variation of temperature is exhibited south of Horseshoe Lake (H) where the land use changes from an urban to a rural fabric. The lower temperatures are recorded over cropland, pasture, and wetland areas. Moreover, the crop and pasture lands (C) north of the city show temperatures ranging from 10°C to 12°C lower than the downtown area. The lowest temperatures are recorded along the Mississippi River where three minima of 29°C are located. A minimum of 31°C is also located over Horseshoe Lake.

3.2.2 August 24 Nighttime Temperatures

The range of nighttime temperatures displayed in Figure 11 is much smaller than the daytime range. Two small areas of 19°C are found along the Mississippi River. Areas of 18°C are found over the

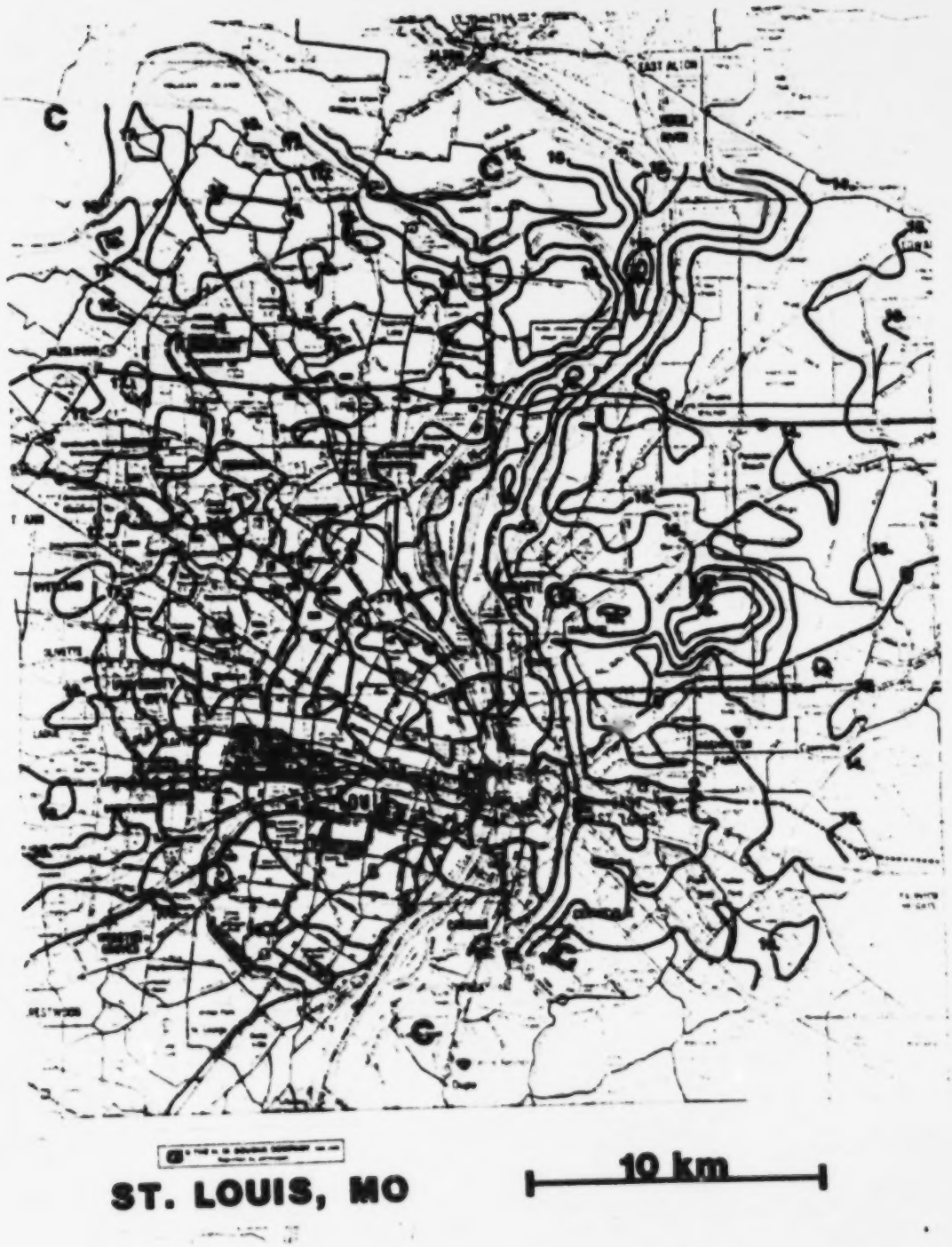

Figure 11. Nighttime blackbody surface temperature analysis for 0230 LST on 24 August 1978 (°C).

downtown area, Horseshoe Lake, Granite City, and East St. Louis. The small 18°C maximum over the northwest corner of the map is associated with a narrow area of commercial activities, as is the small 18°C maximum south of the downtown area. The heat stored during the day in these areas is slowly released at night causing warmer surface temperatures. Duckworth and Sandberg (1954) point out that the heat capacity of urban building materials as compared with that of soil to release stored heat energy during the night is sufficient to account for well over half of most observed urban temperature differences. The rural areas north and east of the city display minima of 14°C to 15°C. However, the model does not include anthropogenic heat effects.

3.2.3 August 23-24 Moisture Availability

The moisture availability (M) values displayed in Figure 12 range from .1 over the urban areas to .7 over some rural areas. Values of M that approach 1.0 are found over the bodies of water.

Minimum values of .1 are found over the downtown area, Granite City, East St. Louis, and the area south of Jennings. This is obviously due to the large areas of concrete and lack of vegetation. Small values of M are also found over some cropland areas where the vegetation is sparse; whereas, larger values of M correspond to more vegetated areas. Forest Park (P), just east of the downtown area, displays a value of .3. Larger values of M are located here but smoothing of the data reduced the displayed value. This is one of the largest municipal parks in the nation,

Figure 12. Moisture availability analysis for 23-24 August 1978.

ORIGINAL PAGE IS
OF POOR QUALITY

so its size of 1400 acres should show up with a somewhat higher value of M than the areas of concrete surrounding it. The maximum value of .8 over Monsenthein Island, northwest of Granite City, is due to the fact that a dense canopy of deciduous trees is prevalent here.

Moisture availability is inversely related to the daytime temperature. For example, .1 corresponds with the 43°C daytime isotherm; similarly, .8 corresponds with the two 29°C isotherms over the Mississippi River and the 31°C isotherm over Horseshoe Lake.

3.2.4 August 23-24 Thermal Inertia

The values of thermal inertia (P) depicted in Figure 13 range from .015 to .07 cal cm^{-2} K^{-1} $s^{-1/2}$. Large values of P are associated with the rivers and Horseshoe Lake; however, the values of P are not reliable over water.

The thermal inertia is closely correlated with the nighttime temperatures. Low values of P (.02-.03) are found north and east of the city over rural areas where the ground does not effectively store heat during the day and does not conduct it to the surface at night. Thus, low nighttime temperatures (14-16°C) correspond with these low values of P. Conversely, high values of P (.04-.05) are found over urban areas near downtown and East St. Louis where there is a high heat capacity of the surface. It is here that the highest nighttime temperatures are found.

Figure 13. Thermal inertia analysis for 23-24 August 1978 (cal cm^{-2} K^{-1} $s^{-1/2}$).

ORIGINAL PAGE IS
OF POOR QUALITY

3.2.5 August 23 Surface Heat Flux

The surface heat fluxes (H_o) shown in Figure 14 correspond to the early afternoon of 23 August. High values of heat flux correspond to high daytime temperatures. Heat flux maxima of 200 Wm^{-2} are found near downtown St. Louis, south of Jennings, and Granite City. These isopleths correspond with the 45°C daytime isotherms. East St. Louis also displays a large heat flux of 180 Wm^{-2} which corresponds to the 43°C daytime isotherm. Conversely, low values of heat flux correspond with low daytime temperatures. Heat flux minima of 60 Wm^{-2} are found over Horseshoe Lake and the Mississippi River. These isopleths conform with minimum daytime temperatures of 29°C to 31°C.

This variability of heat flux with land use corroborates the findings made by Ching et al. (1978). In their study, sensible heat fluxes were calculated by the eddy correlation method. During the summer, the heat flux was found to be largest at a site composed mainly of paved areas and other dry surfaces. Figure 14 shows that the largest heat fluxes in downtown St. Louis and south of Jennings are found over interstate highways which traverse northwest from the city. Ching et al. (1978) also found smaller heat fluxes over more vegetated urban sites with active evapotranspiration.

High H_o values (200 Wm^{-2}) also correspond to low values of M (.1); likewise, low H_o values (60 Wm^{-2}) correspond to high values of M (.8).

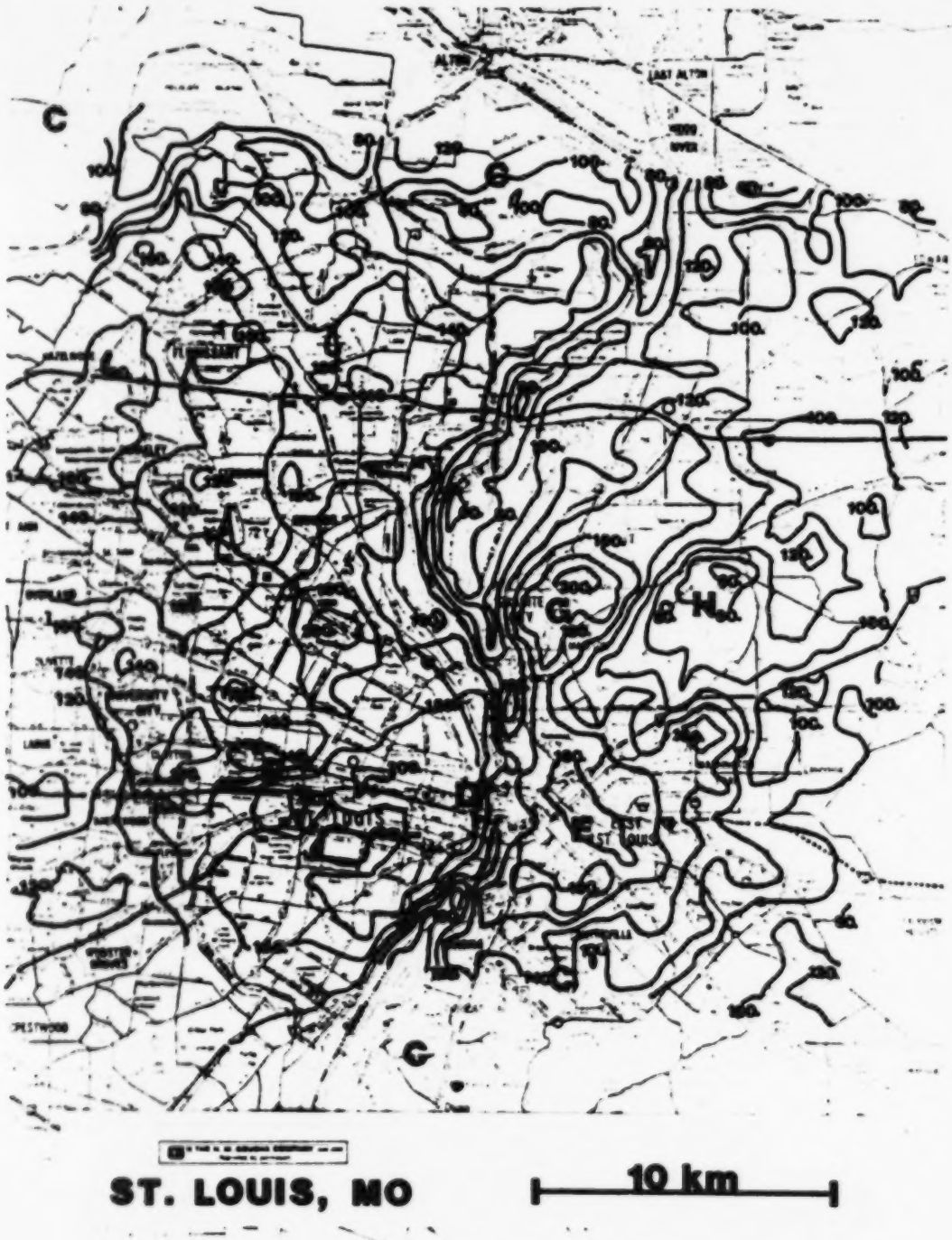

Figure 14. Surface heat flux analysis for the early afternoon of 23 August 1978 (Wm^{-2}).

3.2.6 August 23 Surface Evaporative Heat Flux

The values for the evaporative heat flux (E_o) shown in Figure 15 range from 200 Wm^{-2} in the urban areas to 445 Wm^{-2} over the bodies of water and the outlying rural areas. The minimum values of E_o correspond to the minimum values of M (.1) and the maximum values of H_o (200 Wm^{-2}). Likewise, the maximum E_o values correspond to the maximum M values (.8) and the minimum H_o values (60 Wm^{-2}).

Local maxima such as the 305 Wm^{-2} isopleth over Forest Park reflect the transition from concrete to vegetation. Oke (1979b) maintains that the evaporative cooling associated with such surfaces as Forest Park may be significant in providing local amelioration of heat island influences. Outlying areas which contain large amounts of vegetation exhibit E_o values that approach 480 Wm^{-2}.

3.3 Summary of Results

The maximum daytime surface temperatures corresponded to the minimum values of moisture availability and this was found in the center of St. Louis. The maximum nighttime surface temperatures corresponded to the maximum thermal inertia values and this was also found in the urban centers. Thus, it was seen that M and P were very much responsible for the formation of important temperature variations over the urban-rural complex.

Maxima of heat flux and minima of evaporation were also found in the urban center where the maximum daytime surface temperatures were located. The suppression of evaporation on dry surfaces allowed a larger portion of the net radiation to be partitioned into

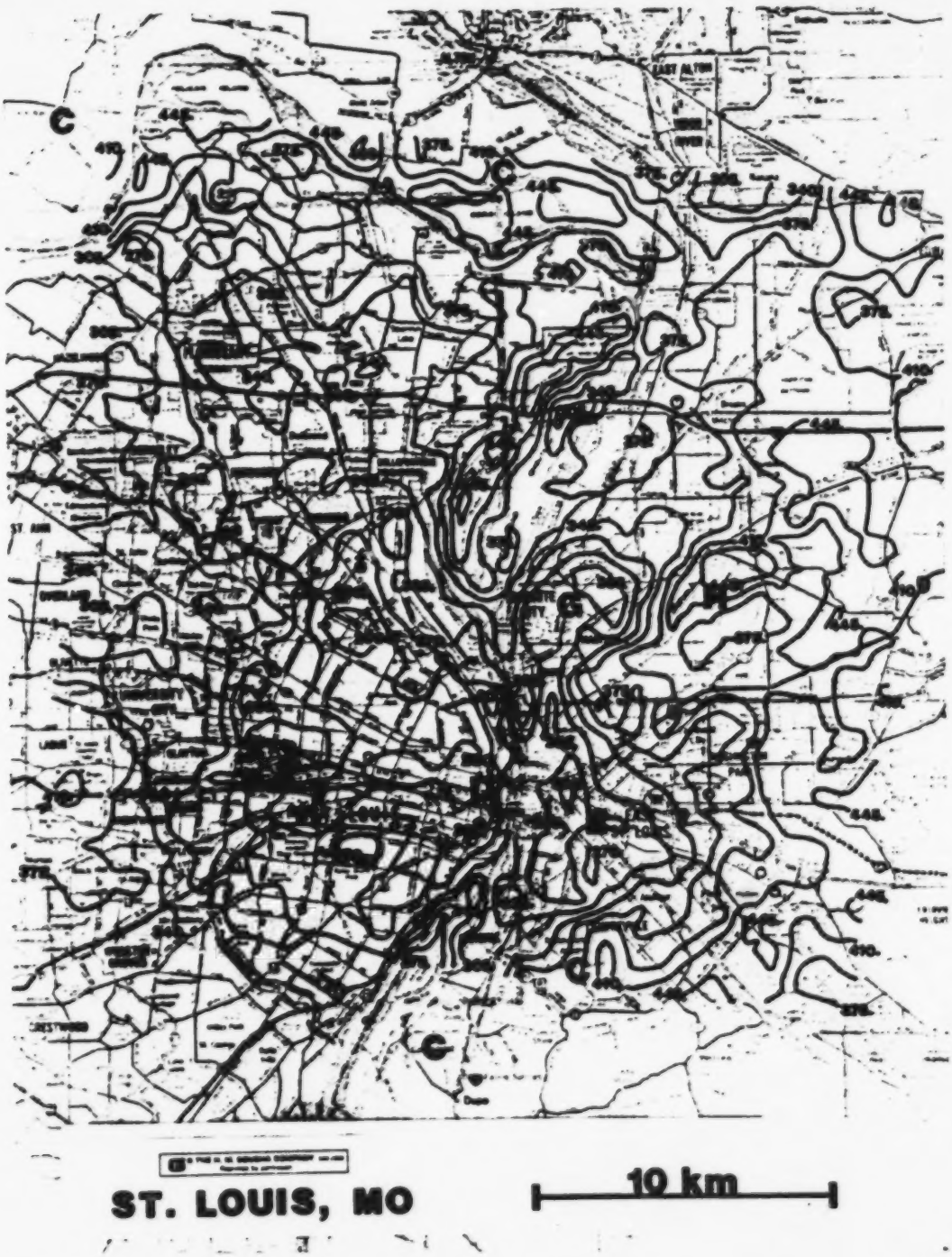

Figure 15. Surface evaporative heat flux for the early afternoon of 23 August 1978 (Wm^{-2}).

ORIGINAL PAGE IS
OF POOR QUALITY

sensible heat, thus causing greater surface heating. The opposite was true for the rural areas. More energy was partitioned into latent heat flux for moist surfaces causing suppressed heating. H_o and E_o were also inextricably tied to the vegetation growth over a particular area. Relatively large heat fluxes and relatively low evaporative heat fluxes were found over areas with little or no vegetation. Low heat fluxes and large evaporative heat fluxes were found over vegetated areas. Hence, a large fraction of the land use variability of heat flux was caused by variability in rates of evapotranspiration, which was caused by the variability of transpiring surfaces.

4.0 PROJECT STATE RESULTS

4.1 Project STATE -- The Tennessee Plume Study

The Environmental Sciences Research Laboratory (ESRL), a division of the EPA's Office of Research and Development (ORD), is conducting various research projects designed to provide data for the development of regional atmospheric deposition models. STATE, an acronym for "Sulfur Transport and Transformation in the Environment", was carried out in 1978 primarily for the purpose of quantifying the impact of various regional sources on air quality.

During August 1978, the STATE program focused on the Tennessee Valley Authority's (TVA) Cumberland power plant in north-central Tennessee. Schiermeier et al. (1979) give the following reasons why the Cumberland steam plant was chosen. First, the power plant already possessed extensive pollutant monitoring facilities and meteorological forecasting data. Also, the site is located within the Sulfate Regional Experiment (SURE) monitoring network. The plant has a generating capacity of 2600 MW with two 1300 MW boilers each connected to its own 305 m stack by three ducts. The three ducts are equipped with two electrostatic precipitators per duct with sampling ports before and after the precipitators. The coal used by the plant is fairly homogeneous and it has an approximately 3% sulfur content. Finally, Cumberland was chosen because it is a base load station which reduces the pollutant emission fluctuations. TVA, other government agencies, universities (including Penn State), and private organizations conducted the field experiments which were

designed to provide information on and insight into the dynamics of plume transport and transformation over long distances.

4.2 Background August 22-23, 1978

The Tennessee Plume Study was conducted in northwestern Tennessee and southwestern Kentucky. Satellite derived measurements of temperature, heat and evaporative fluxes, thermal inertia, and moisture availability were made for two adjacent areas: The Land Between the Lakes, Kentucky, and Clarksville, Tennessee.

In the 1960's, the TVA launched an ambitious project for a national outdoor recreation center located in the Land Between the Lakes. The base map used for the Land Between the Lakes study, along with key areas that have been coded for easy reference, is shown in Figure 16. Kentucky Lake and Lake Barkley are large, artificial lakes formed by the dams of the Tennessee Valley Authority and the U.S. Corps of Engineers. The Land Between the Lakes is a heavily forested area with predominantly deciduous trees.

The base map used for the Clarksville study, along with coded areas, is shown in Figure 17. Clarksville, Tennessee, situated 64 km northwest of Nashville, has a population of approximately 32,000. Situated along the Cumberland River, the city lies in a dark-tobacco, livestock, and farming region. Clarksville is a leading marketing center for tobacco products, shoes, and clothes. Fort Campbell, 14 km northwest of Clarksville, is on the Tennessee-Kentucky border. This U.S. army post, which has a population of approximately 23,000, is the home of the 101st Airborne Division.

Figure 16. The base map used for the Land Between the Lakes case study along with the following key areas coded for easy reference:

LBL Land Between the Lakes

KL Kentucky Lake

JC Jonathan Creek

BR Blood River

LB Lake Barkley

LR Little River

DC Donaldson Creek

NSP Numerous Small Ponds

FCR Fort Campbell Restricted Area

F Forest and Brushwood

C Cropland and Pasture

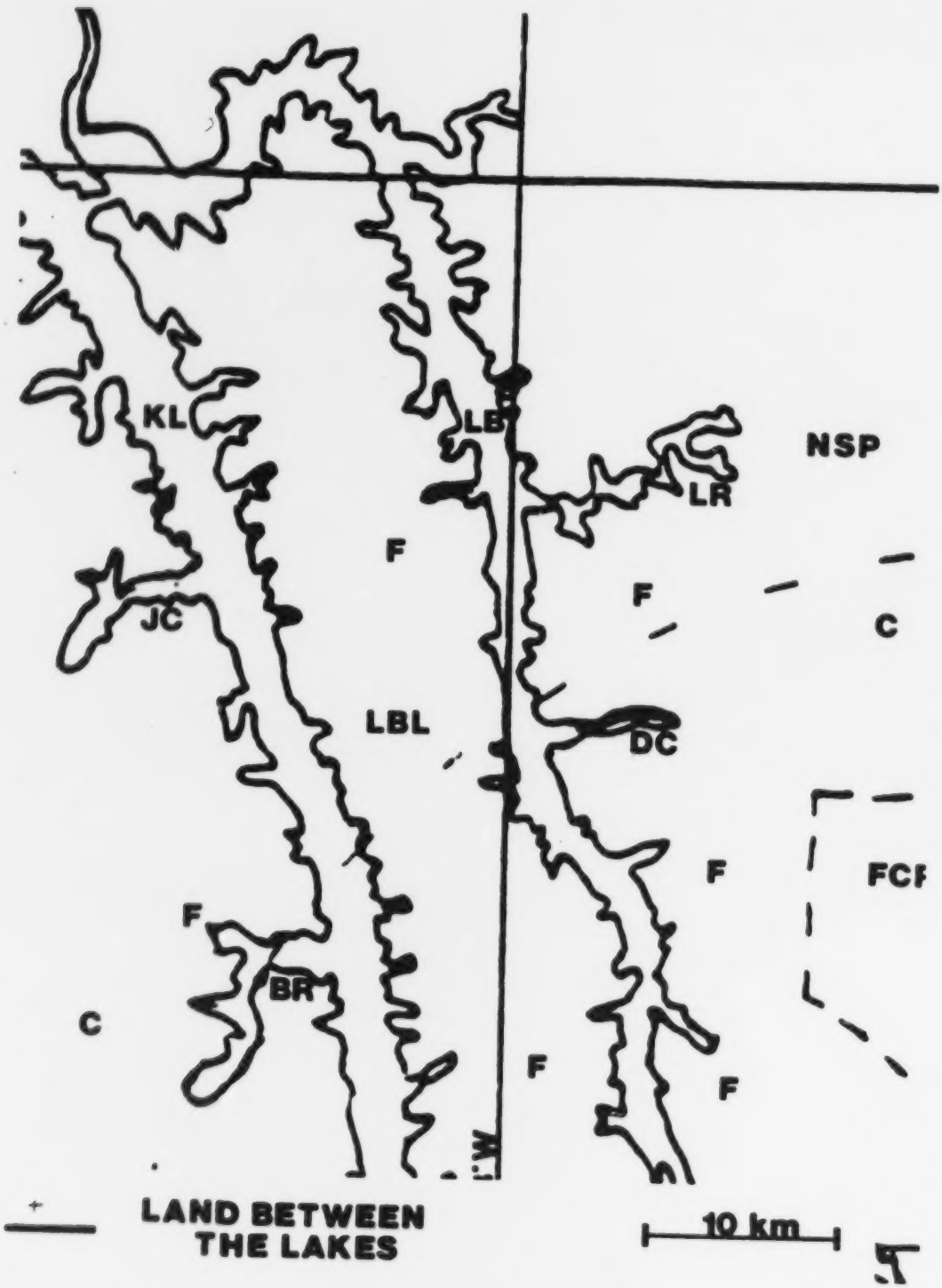
KL
LB
NSP
LR
F
F
C
JC
LBL
DC
F
FCF
F
BR
C
F
F
LAND BETWEEN
THE LAKES
10 km

Figure 17. The base map used for the Clarksville case study along with the following key areas coded for easy reference:

CR Cumberland River

HP Hickory Point

WL Woodlawn

CB Corbandale

FCR Fort Campbell Restricted Area

NC Numerous Creeks

NSP Numerous Small Ponds

F Forest and Brushwood

C Cropland and Pasture

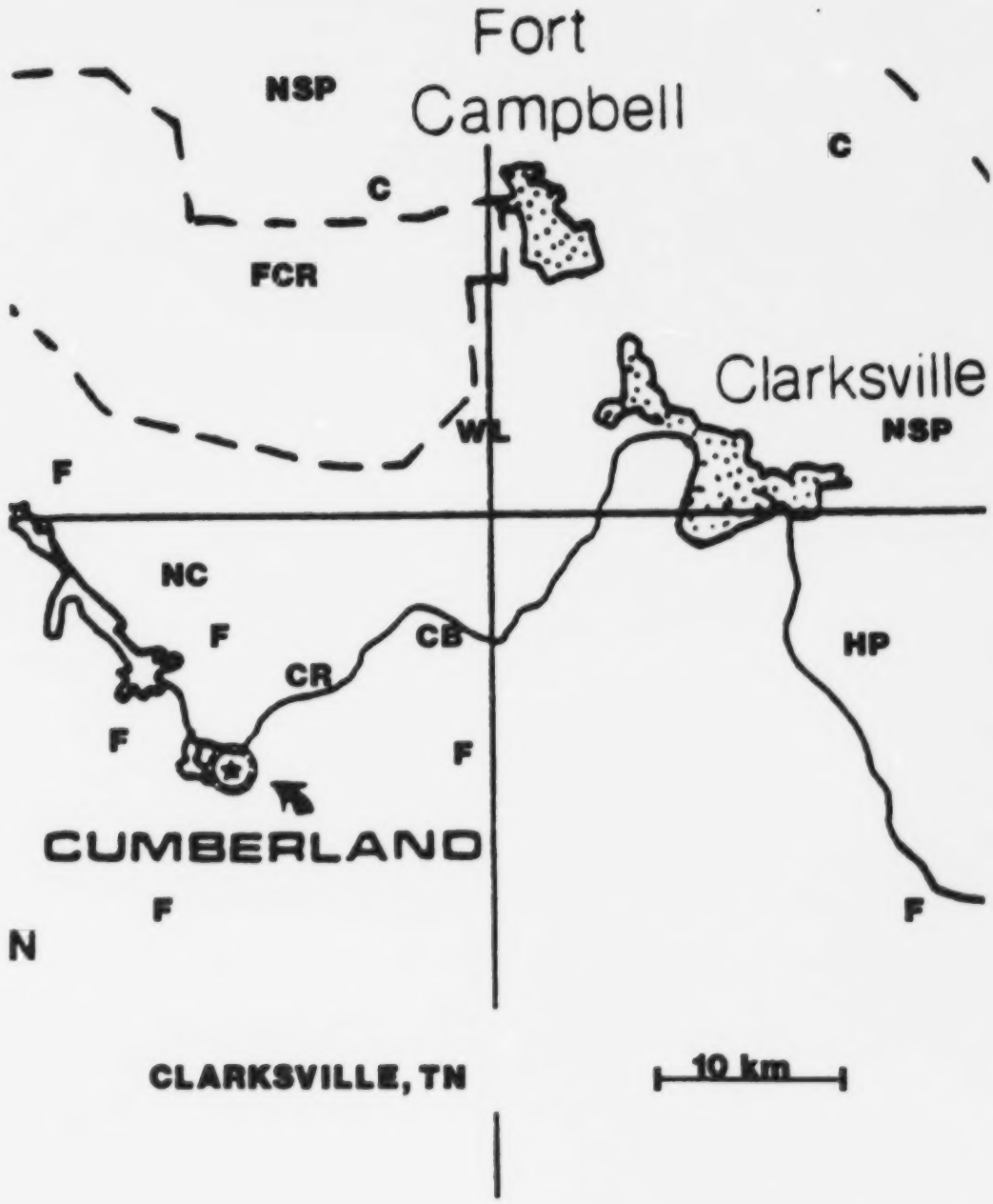
Fort
Campbell
NSP
C
C
FCR
Clarksville
NSP
WL
F
NC
F
CB
CR
HP
F
F
CUMBERLAND
F
F
N
CLARKSVILLE, TN
10 km

The Fort Campbell restricted zone encompasses over 100,000 acres. Except for the restricted area and the forested region, tobacco and general farming dominate the area around Fort Campbell and Clarksville.

A high pressure system centered over northern West Virginia produced generally clear skies on 22-23 August 1978. The daytime temperatures were around 31°C and the nighttime temperatures averaged about 14°C over the region. No significant precipitation had occurred in the area for at least a week.

The satellite images were taken twelve hours apart on 22 August 1978 at approximately 0300 LT and 1400 LT. The model output was for 1400 LT on 22 August and 0300 LT on 23 August. This reversal of orbit times is justified because it is believed that the temperature response between the two days was stationary.

Table II lists some of the initial parameters used for the Land Between the Lakes and Clarksville model runs. The 1200 GMT Johnsonville, Tennessee soundings for 22 and 23 August 1978 were averaged. The average sounding, shown in Figure 18, was used as input to the boundary layer model. The average sounding was believed to be more representative of the two days.

4.3 The Land Between the Lakes August 22-23, 1978

4.3.1 August 22 Daytime Temperatures

A 12°C variation of daytime surface temperatures is evident in Figure 19. The maximum temperature (36°C) is located just west of the Blood River (BR) which is only 26°C. This variation in

Table II. Initial Model Input Parameters for Land Between the Lakes and Clarksville

Ground Temperature at the Base of the Layer	287°K
Roughness Length	25 cm
Precipitable Water	1.88 cm
Albedo	.19
Emissivity	1.0
Wind Speed at z $\sim$ 3 m	5.8 $msec^{-1}$
Direction	45°

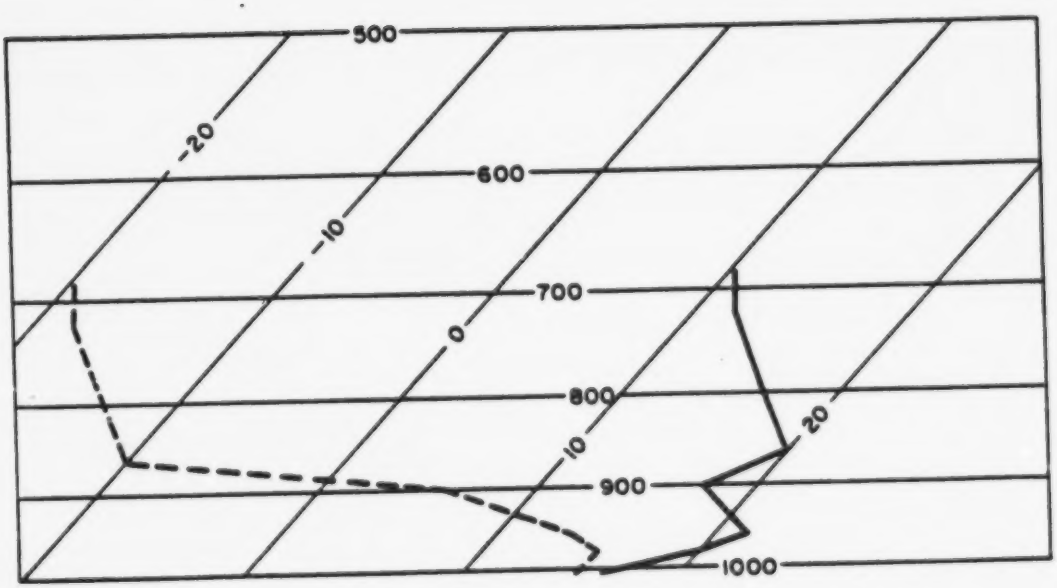

Figure 18. The 1200 GMT Johnsonville, TN average sounding for 22 and 23 August 1978.

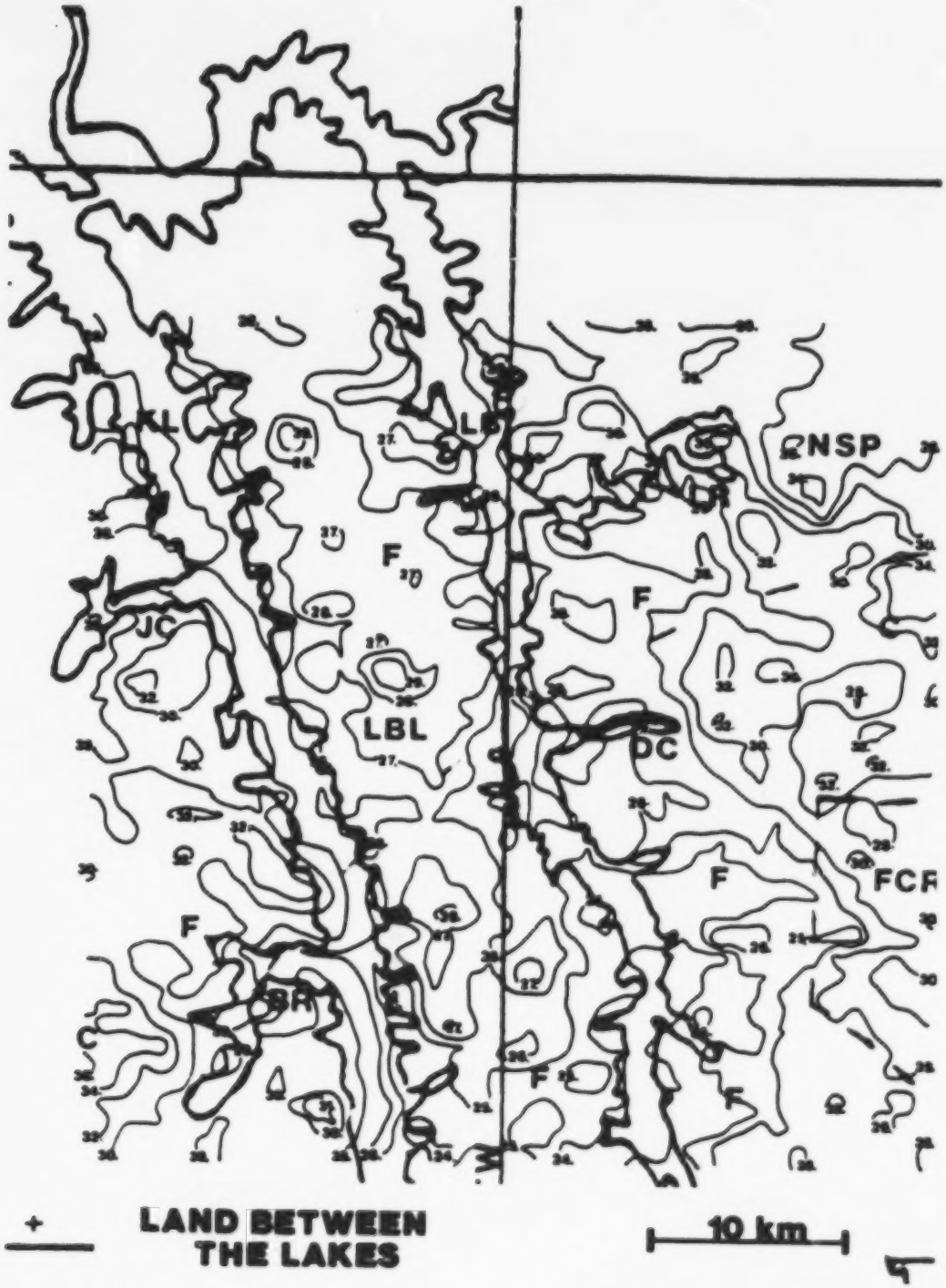

Figure 19. The Land Between the Lakes daytime blackbody surface temperature analysis for 1400 LT on 22 August 1978 (°C).

temperature is in direct response to a change of land use, close cropped vegetation or urban areas to highly vegetated or well-watered surfaces. The lower temperatures are recorded over the river and the forested areas (F); whereas, the highest temperatures are found over the croplands (C). Temperatures greater than 29°C are found east of the Blood River, south of Jonathan Creek (JC) where there is some cropland crossed by a state highway, southeast of the Little River (LR) over farmland, and in the central part of the Land Between the Lakes where the town of Golden Pond lies. Golden Pond is a town with fewer than 1,000 inhabitants, so it's astonishing that a temperature maximum is observed. The 32°C isotherm south of the Little River is associated with the town of Cadiz and the intersection of two major highways. Cadiz has a population of about 2,500 people; however, an intense temperature maximum is not observed here because some cloud (cirrus) was located in that region, though the cloud was removed from the analysis by replacing cloud pixel values with those of neighboring clear sky pixels. The two areas of 30°C north of the Little River (LR) conform to patches of cleared areas in the forest. The three 32°C isotherms north of the Fort Campbell (FC) border are associated with two interstate highways. The three 32°C isotherms north of the Blood River (BR) are closely connected with the areas that have been cleared in the forest for highways. Temperatures ranging from 24°C to 29°C are found over the Land Between the Lakes which is a predominantly forested area.

The lowest temperatures are found over the bodies of water where minima of 24°C are found over Kentucky Lake (KL), Lake Barkley (LB), and the numerous small ponds (NSP).

4.3.2 August 23 Nighttime Temperatures

The nighttime surface temperatures shown in Figure 20 range from 11°C to 23°C. Isotherms valued at 20°C to 23°C are found over Kentucky Lake and 18°C to 21°C isotherms are found over Lake Barkley, compared with 24°C to 28°C daytime temperatures. Thus, the diurnal temperature variation over water surfaces is small. Oke (1978) gives the following reasons why water exhibits very little thermal response. Water allows short-wave radiation to be transmitted to considerable depths and the existence of convection and mass transport by the fluid motions permits the absorbed heat to be spread throughout a large volume. Also, the unlimited water availability provides an efficient latent heat sink, and evaporative cooling tends to destabilize the surface layer and further enhance mixing. Finally, the thermal capacity of water is exceptionally large. In fact, about three times as much heat is required to raise a unit volume of water through the same temperature interval as most soils.

The nighttime temperatures over the Land Between the Lakes range from 13°C to 14°C. The croplands exhibit 12°C to 13°C temperatures and an 11°C minimum is observed in the Fort Campbell restricted area.

4.3.3 August 22-23 Moisture Availability

The isopleths of moisture availability shown in Figure 21 are largest over the dense canopy of trees which predominate the Land Between the Lakes region. M approaches 1.0 over a large portion of this region. The three minima of .6 located south of Jonathan

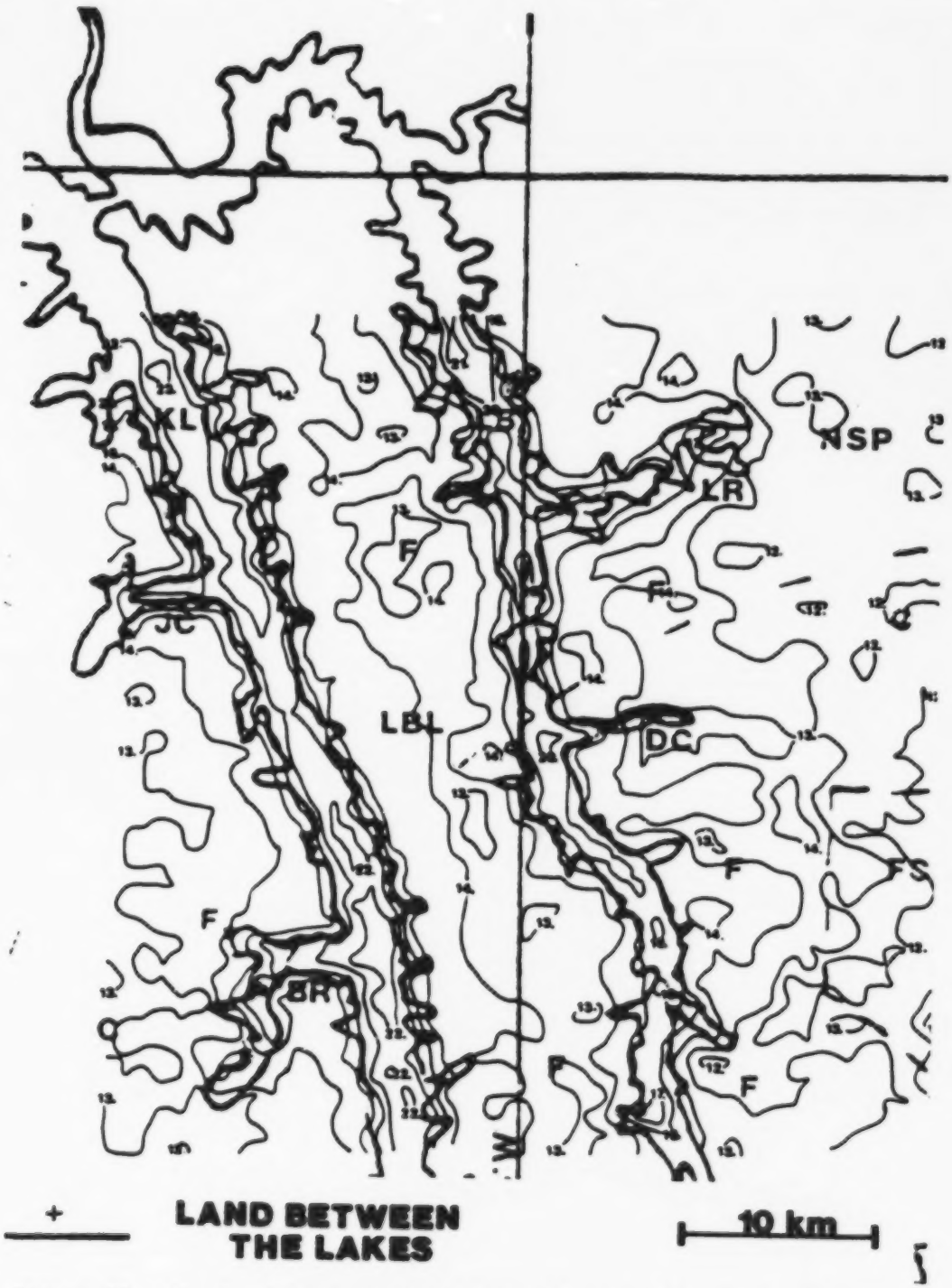

Figure 20. The Land Between the Lakes nighttime blackbody surface temperature analysis for 0300 LT on 23 August 1978 (°C).

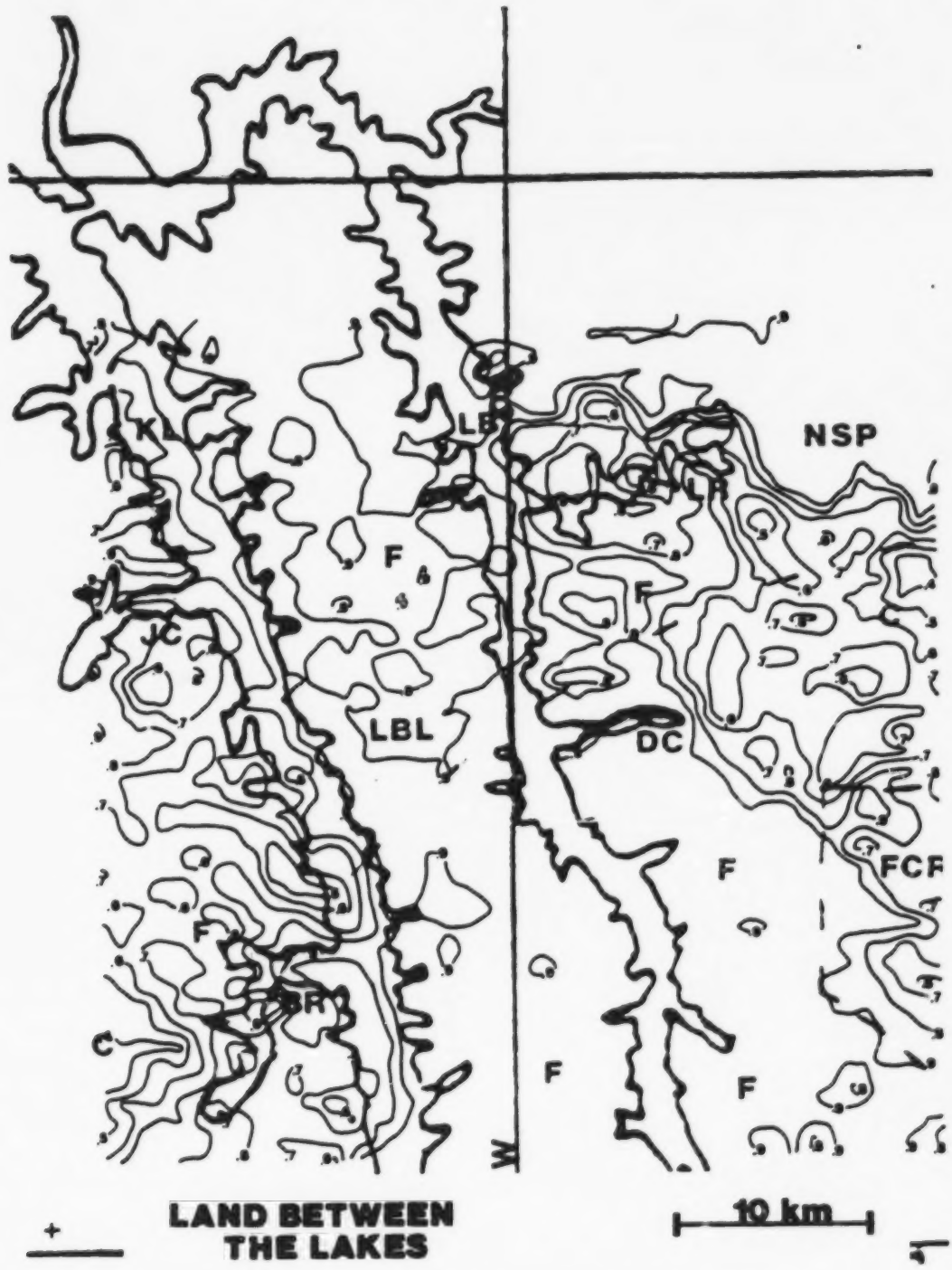

Figure 21. The Land Between the Lakes moisture availability analysis for 22-23 August 1978.

Creek (JC) are associated with a state highway and cropland. The .5 and .6 isopleths located north of the Blood River (BR) correspond to previously forested areas that had been cleared. Values of .7 are found over the southwestern portion of the Blood River and M is .4 about two kilometers west of the river. Another large variation of M with land use is found southeast of the Little River (LR) where M varies from .8 to .4 over a distance of four kilometers. The non-forested, open areas of Fort Campbell also reflect the lower moisture availability values. M varies from .6 to .8 in this area.

Comparing the daytime surface temperatures with moisture availability, one can see the inverse relationship between these two variables. The highest daytime temperatures correspond to the lowest values of M. For example, the 34°C to 36°C isotherms west of the Blood River correspond to the .4 isopleth of M. Conversely, the 24°C to 25°C isotherms over the southern portion of the Land Between the Lakes correspond to values of M that approach 1.0.

4.3.4 August 22-23 Thermal Inertia

The values of thermal inertia depicted in Figure 22 range from .03 to values which are greater than .07. The elimination of values greater than .07 in the analysis tends to remove detail around the lakes where P exceeded .07. The values of P range from .05 to .07 over the predominantly forested Land Between the Lakes. The .04 minimum south of Jonathan Creek (JC) corresponds to the state highway and cropland. The crop and pasture land west of the Blood River (BR) and north of Fort Campbell (FC) display values of .03. Isopleths of .06 are found over the numerous small ponds (NSP)

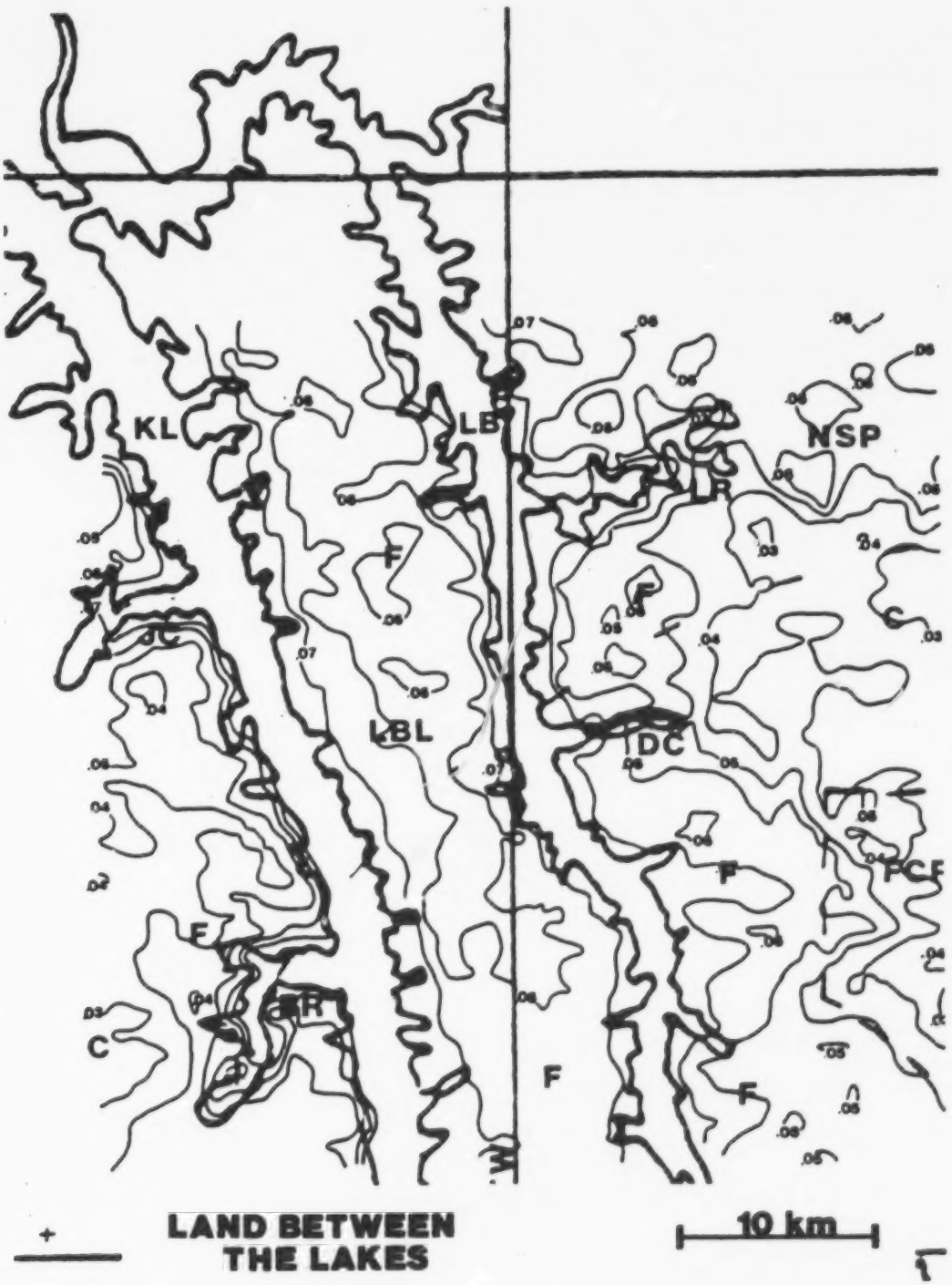

Figure 22. The Land Between the Lakes thermal inertia analysis for 22-23 August 1978 (cal cm^{-2} K^{-1} $s^{-1/2}$).

east of the Little River. The non-forested, open areas of Fort Campbell display values between .03 and .06.

The .05 to .06 values of P located over the Land Between the Lakes correspond to nighttime temperatures of 13°C and 14°C. The highest nighttime temperatures occur over regions where the highest thermal inertia values are observed, such as Kentucky Lake and Lake Barkley. The largest diurnal temperature change is found where the thermal inertia is at a minimum. For example, the .03 minimum P value over the cropland west of the Blood River corresponds to a 23°C diurnal temperature variation.

4.3.5 August 22 Surface Heat Flux

The surface heat flux values, shown in Figure 23, are lowest over the bodies of water and the forested areas. H_o varies from 35 Wm^{-2} to 95 Wm^{-2} over the Land Between the Lakes. The local maximum H_o (95 Wm^{-2}) value located over the central portion of the Land Between the Lakes corresponds to the small town of Golden Pond. The local maximum (135 Wm^{-2}) south of Jonathan Creek (JC) is associated with a state highway. The local maximum (155 Wm^{-2}) north of the Blood River (BR) conforms to previously forested areas that had been cleared for highways. The largest heat flux values (175 Wm^{-2}) are found over the closely cropped vegetation west of the Blood River and north of Fort Campbell (FC). The 135 Wm^{-2} isopleth south of the Little River (LR) is associated with Cadiz. The numerous small ponds (NSP) east of the Little River display values of 35 Wm^{-2}, with a 15 Wm^{-2} minimum over one of the larger ponds.

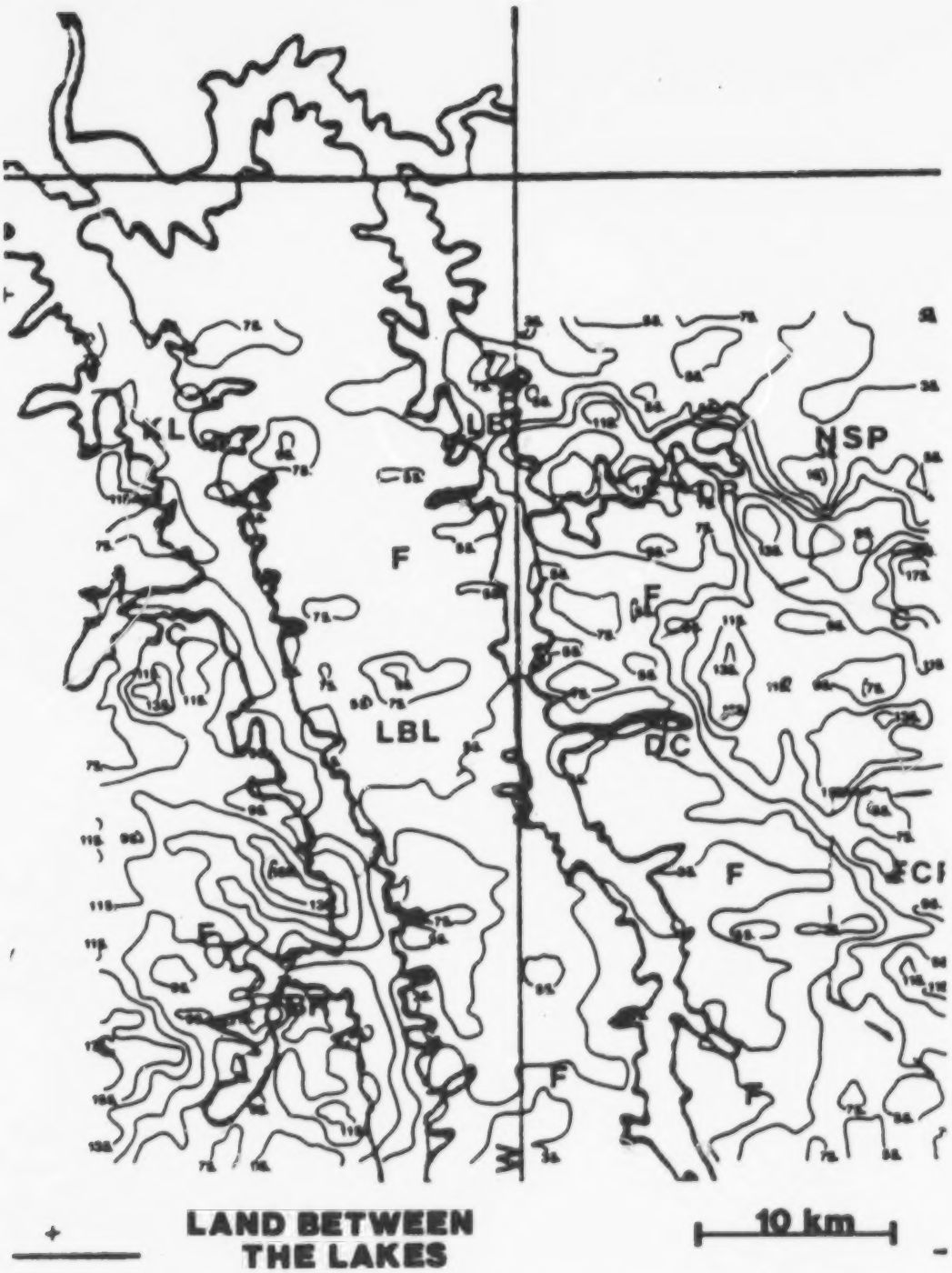

Figure 23. The Land Between the Lakes surface heat flux analysis for the early afternoon of 22 August 1978 (Wm^{-2}).

4.3.6 August 22 Surface Evaporative Heat Flux

The isopleths of the surface evaporative flux, shown in Figure 24, range from 290 Wm^{-2} to 610 Wm^{-2}. The largest values of E_o are found over the dense forest canopy where moisture is absorbed through the roots of the many trees and then transpired. Budyko (1963) estimates the relative value of transpiration to represent 30 to 40 percent of the total evaporation even for relatively low vegetative covers, such as grass at a height of 10 to 20 cm. The relative value of transpiration is presumably even greater from the soil in a forested area. Spittlehouse and Black (1979) used Bowen ratio and eddy correlation measurements to determine the evapotranspiration of a forest. They found evaporation rates corresponding to values of M that exceeded .5.

Lower evaporative flux values (490 Wm^{-2}) are found south of Jonathan Creek (JC) over a state highway, south of the Little River (LR) over Cadiz, and east of Donaldson Creek (DC) over a highway. H_o values varying from 410 Wm^{-2} to 450 Wm^{-2} are found over farmland. Evaporative flux minima are found over Kentucky Lake and Lake Barkley because of the cool daytime surface temperatures.

The largest E_o values are found over regions where H_o was at a minimum and M was at a maximum. Reginato et al. (1976) experimented with Avondale loam and found that when the soil water content is high, the hydraulic conducting property of the soil is relatively high, thereby allowing enough water to flow to the soil surface to meet the meteorological demand of the potential evaporation rate. When the soil water diminishes below a certain value (i.e. second stage

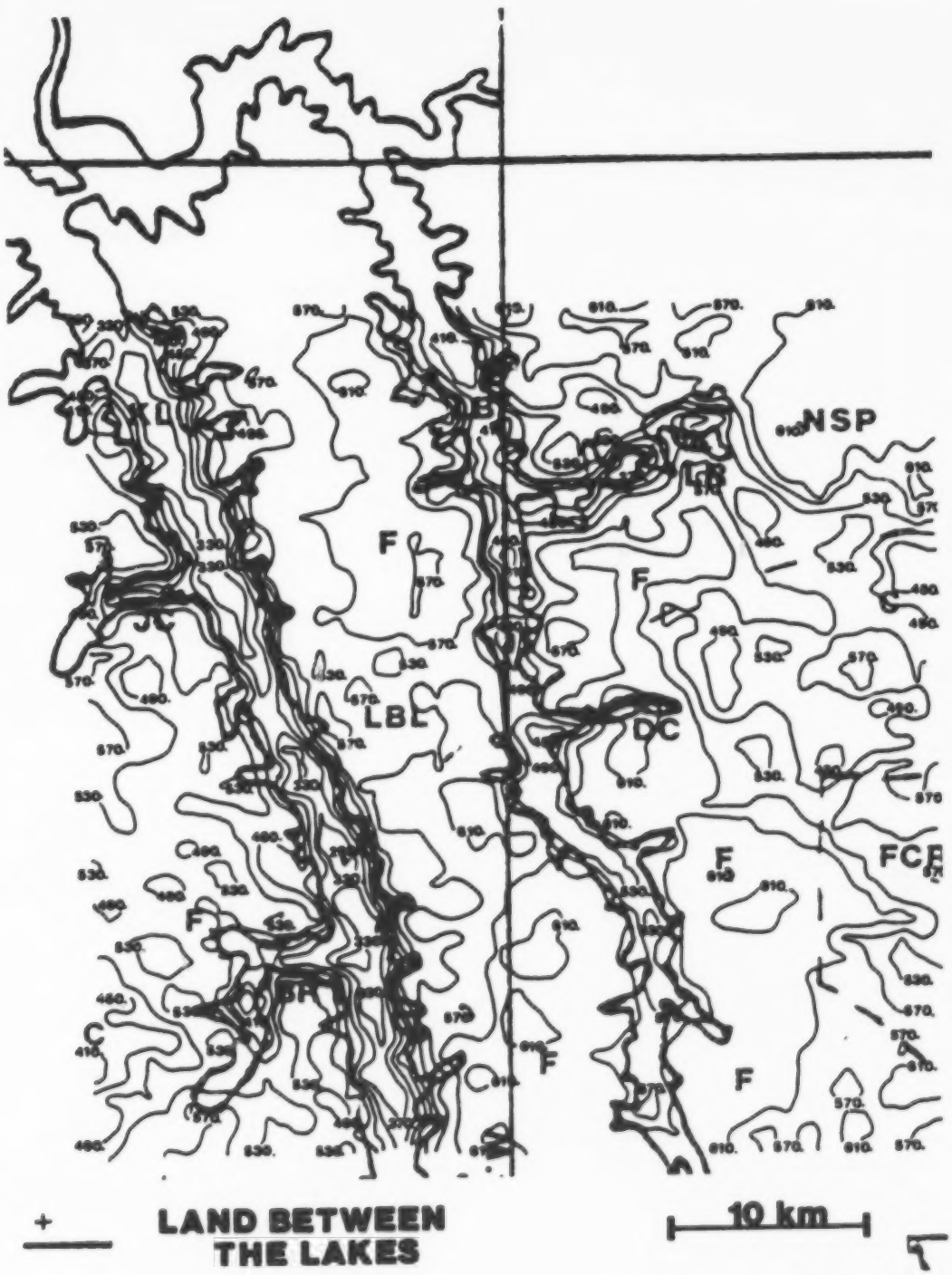

Figure 24. The Land Between the Lakes surface evaporative heat flux analysis for the early afternoon of 22 August 1978 (Wm^{-2}).

ORIGINAL PAGE IS
OF POOR QUALITY

of drying), the potential evaporation rate cannot be met, and the relative evaporation rate declines with the decreasing water content.

4.4 Clarksville August 22-23, 1978

4.4.1 August 22 Daytime Temperatures

The isotherms depicted in Figure 25 range from 36°C to 23°C. The warmest area is Clarksville where the temperature varies from 26°C over the southeastern corner of the city to 36°C over the northwestern portion. Fort Campbell displays a temperature maximum of 33°C. Three very small towns, all with populations of fewer than 1,000 people, are referred to in the key because, surprisingly, they display temperature maxima. Woodlawn (WL) and Corbandale (CB) display temperature maxima of 30°C and Hickory Point (HP) displays a maximum surface temperature of 33°C.

Minimum surface temperatures are found over forested areas and wetlands (F). In these regions, the temperature varied from 23°C to 28°C. The temperature over the numerous small ponds (NSP) and numerous creeks (NC) varied from 26°C to 28°C. Cropland and pasture areas (C) exhibit temperatures which range from 28°C to 30°C with a few 26°C minima.

4.4.2 August 23 Nighttime Temperatures

The nighttime temperatures displayed in Figure 26 show a 5°C variation across the area. The maximum temperature (15°C) is found over the numerous small ponds (NSP) and creeks (NC) that are prevalent

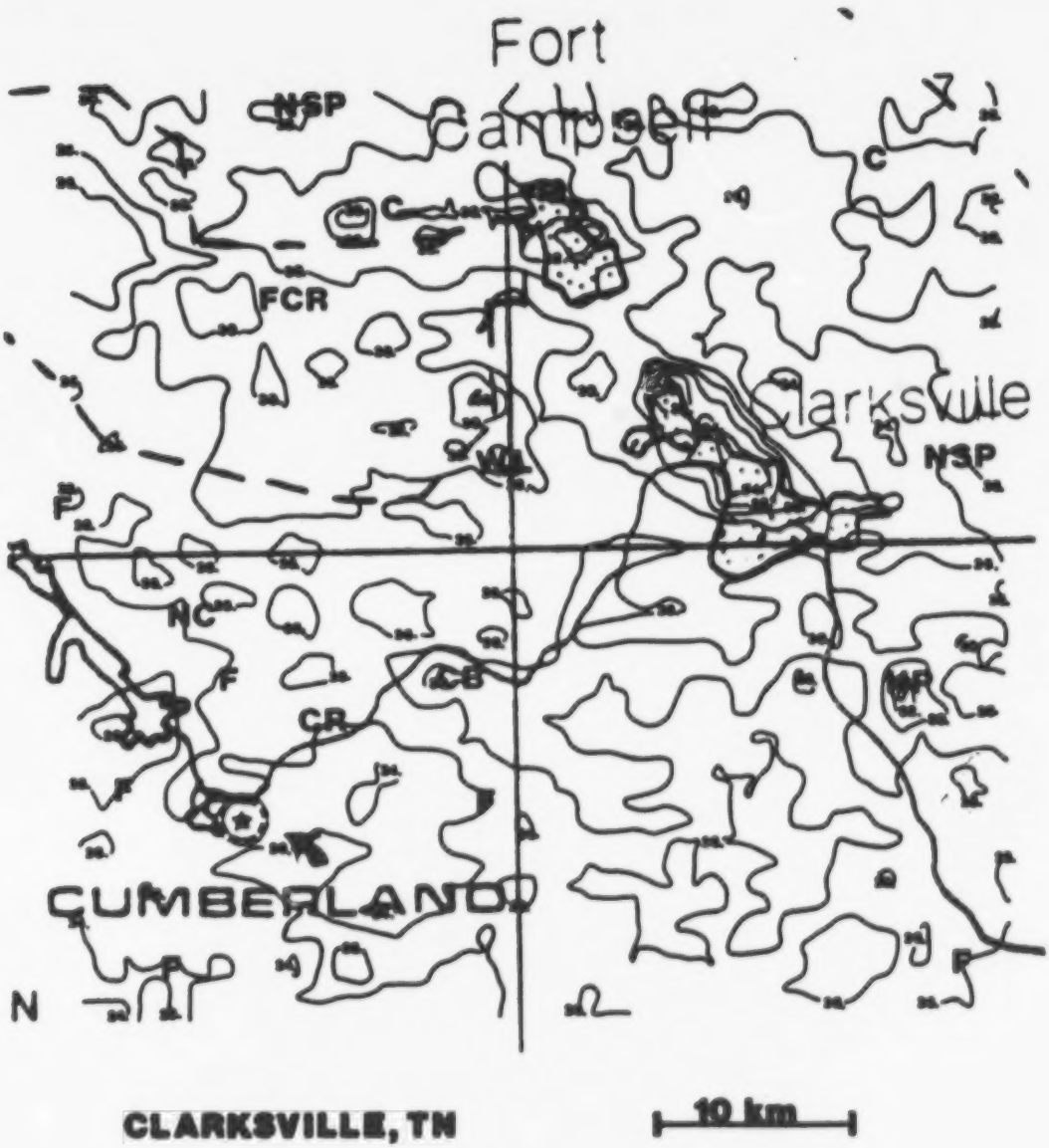

Figure 25. The Clarksville blackbody daytime surface temperature analysis for 1400 LT on 22 August 1978 (°C).

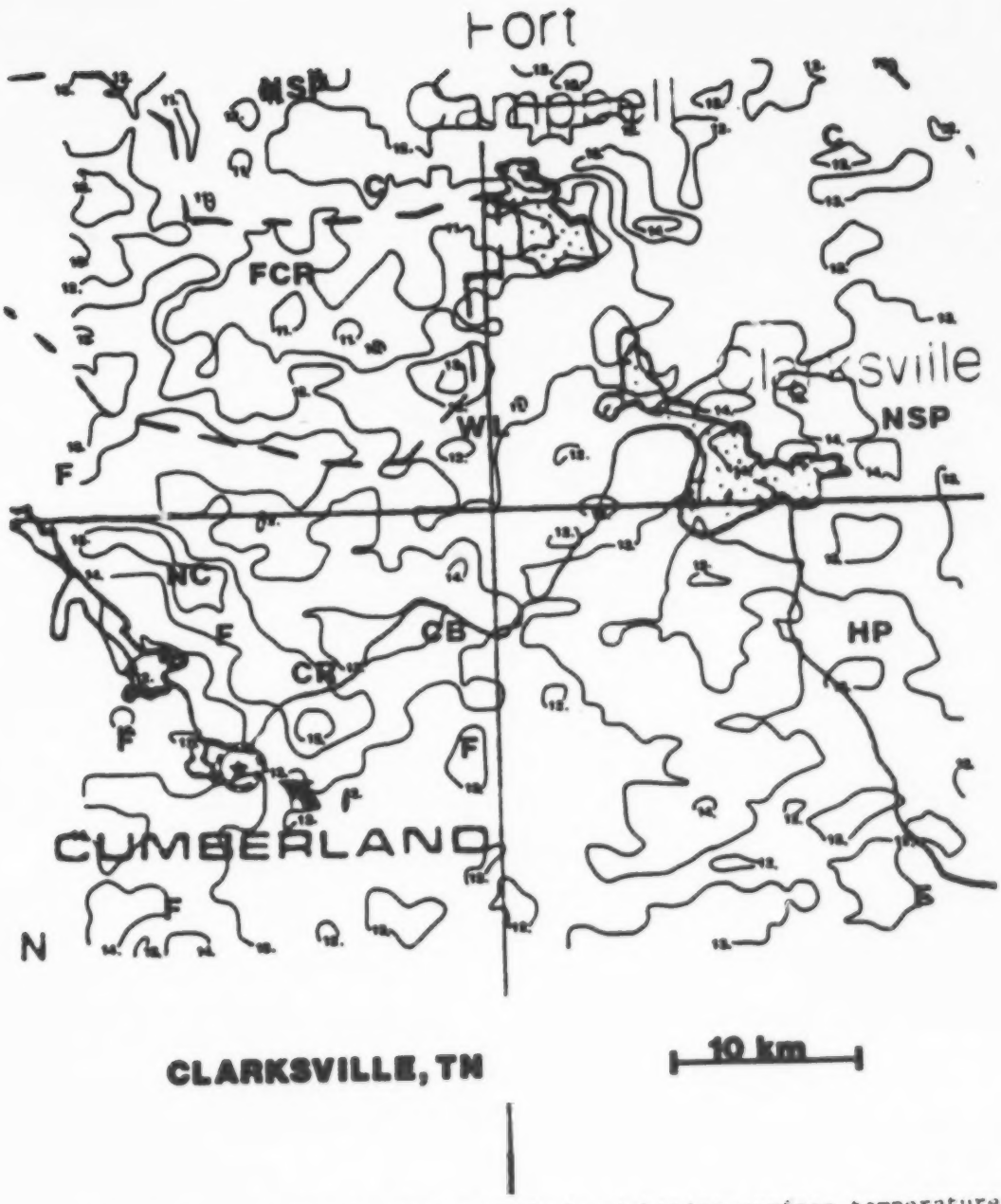

Figure 26. The Clarksville blackbody nighttime surface temperature analysis for 0300 LT on 23 August 1978 (°C).

in this part of Tennessee. The only urban area that shows some sort of heat island is Clarksville where the temperature is 14°C. Fort Campbell does not display elevated temperatures because this is a military installation with no factories or industrial areas which are important contributors to the nighttime urban heat island. The Fort Campbell restricted area (FCR) shows a localized 10°C minimum because of the bare ground found here. The forested areas display temperatures ranging from 12°C to 14°C, and 11°C to 12°C minima are found over closely cropped vegetation where the soil maintains a low heat capacity.

4.4.3 August 22-23 Moisture Availability

The wide range of moisture availability, found in Figure 27, is indicative of varied land use. The highest values of M are found over the forested areas (F) and over the numerous small ponds (NSP) and creeks (NC) where M approaches 1.0. Clarksville shows a sharp variation of M from .9 over the outskirts of the city to .4 over the inner portions of the city. Corbandale and Woodlawn show minima of .7, and Fort Campbell and Hickory Point both display .5 minima. The Fort Campbell restricted area (FCR), a non-forested area, displays values ranging from .6 to .9 depending on the amount and type of vegetation that were present. High values of M are found over the densely vegetated crops northeast of Clarksville; however, the values were much lower over the croplands west of Fort Campbell. This reflects how M varied with the type of crop grown and the amount of irrigation that was done.

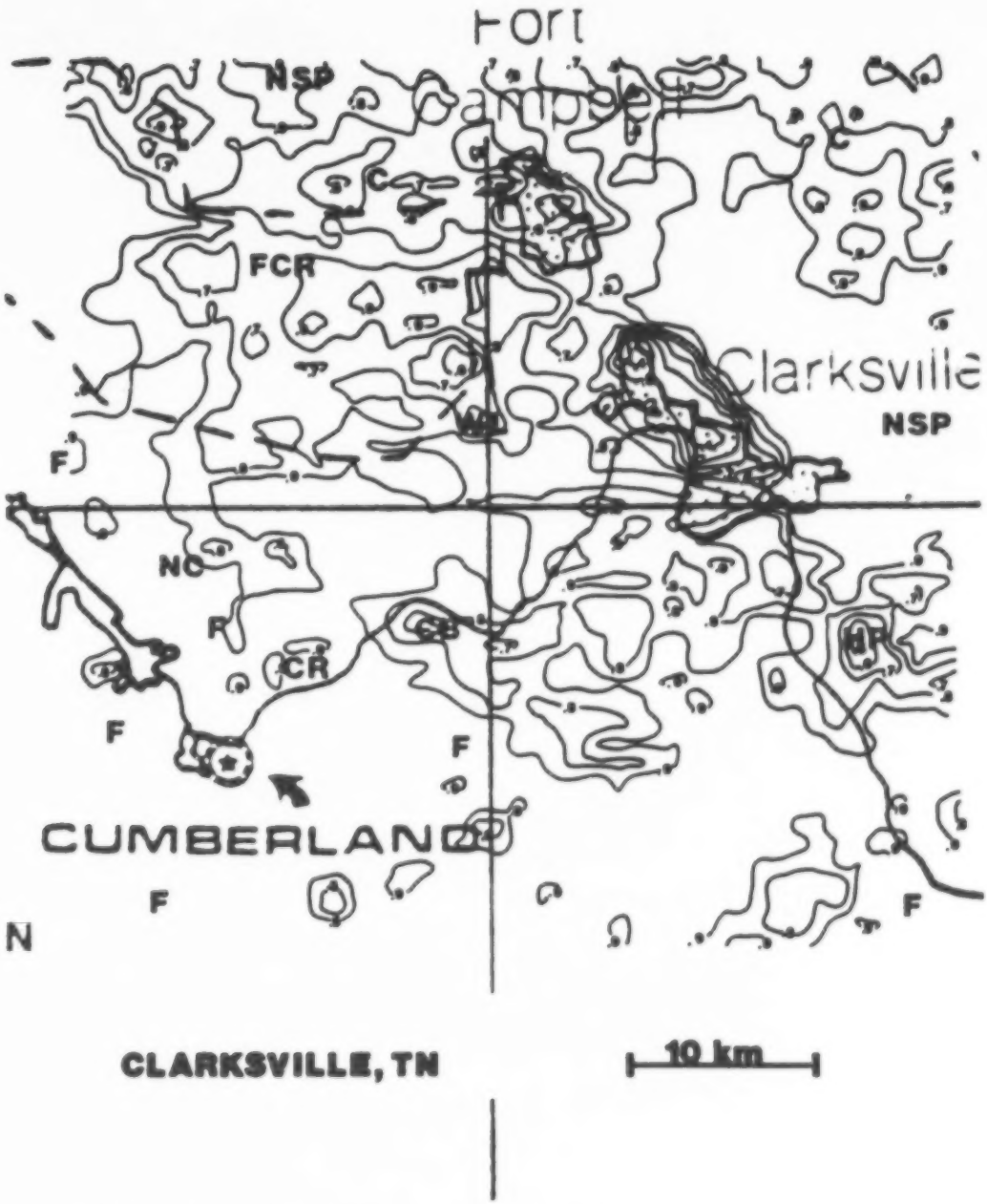

Figure 27. The Clarksville moisture availability analysis for 22-23 August 1978.

The negative correlation between daytime temperatures and moisture availability is again evident. The .4 minima over Clarksville correspond to the 34°C and 36°C maximum daytime isotherms (Figure 25); likewise, the .5 minima over Fort Campbell and Hickory Point (HP) correspond to the 33°C maximum isotherms. Conversely, the lowest temperatures on the map (23°C) correspond to values of M that approach 1.0.

4.4.4 August 22-23 Thermal Inertia

The thermal inertia values shown in Figure 28 vary from .02 to .07. The lowest values of P, surprisingly, are found over the urban areas. One would anticipate a maximum of P over the urban areas which would reflect the enhanced ability of the urban substrate to store and conduct heat. However, minimum values of .02 are found over Clarksville and Fort Campbell. Low thermal inertia values were also found by Dodd (1978) over urban areas. Hickory Point (HP) and Woodlawn (WL) display values of .03, and Corbandale (CB) shows a higher value of .04. The forests display thermal inertia values ranging from .05 to .07.

Thermal inertia varied in a similar manner to the nighttime temperature pattern. The large values of P (.06-.07) corresponded to the maximum nighttime temperatures (14-15°C). Low values of P are found over Clarksville, Fort Campbell, and the other small towns; because of the low values of P there, no significant increase in nighttime temperatures is found for these urban areas.

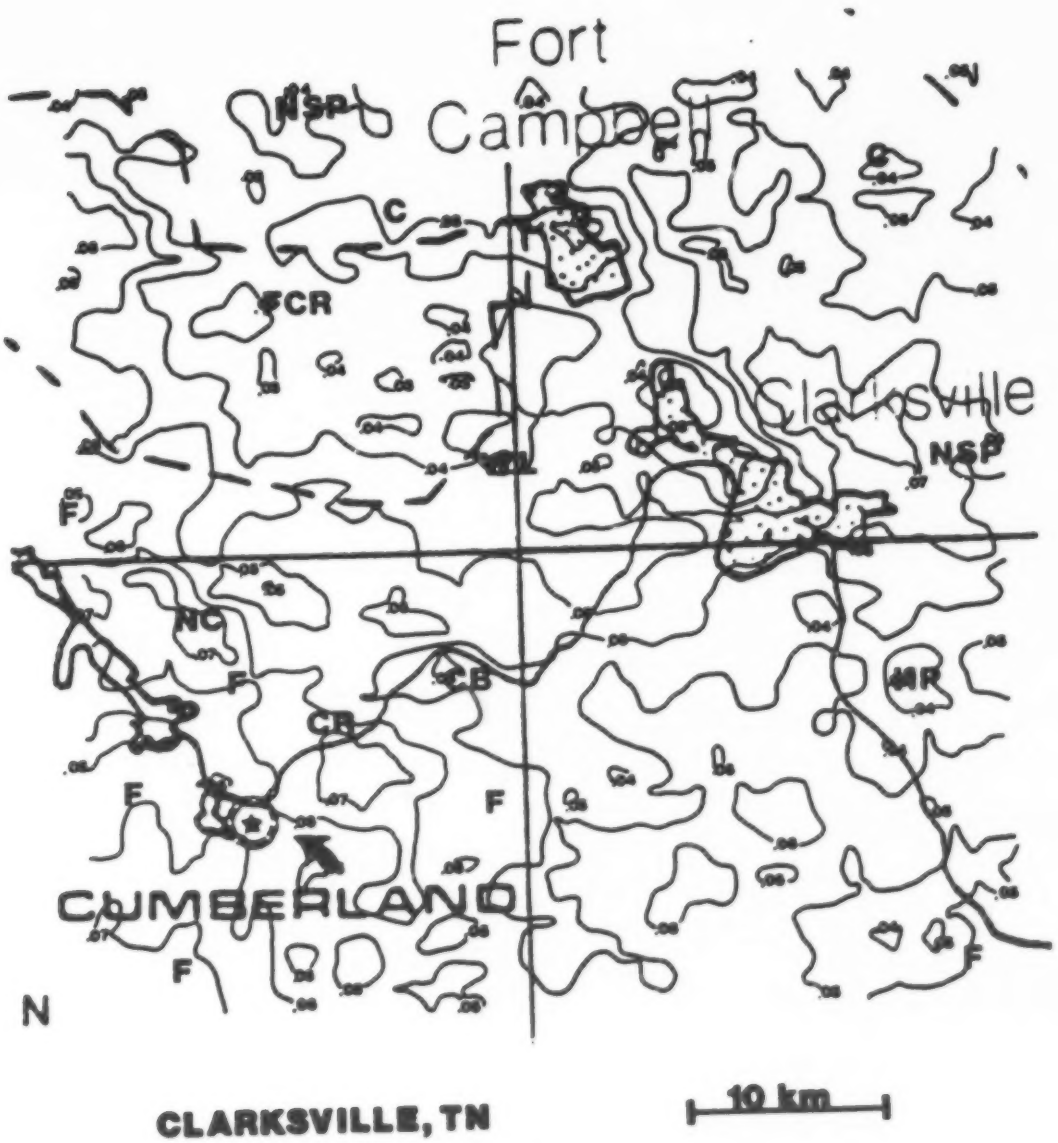

Figure 28. The Clarksville thermal inertia analysis for 22-23 August 1978 (cal cm^{-2} K^{-1} $s^{-1/2}$).

4.4.5 August 22 Surface Heat Flux

Figure 29 shows a wide variation of the surface heat flux with land use. The largest values of H_o are found over Clarksville (170 Wm^{-2}), Fort Campbell (150 Wm^{-2}), Hickory Point (130 Wm^{-2}), and Woodlawn (110 Wm^{-2}). These areas correspond to the maximum daytime isotherms and minimum values of moisture availability. Heat flux minima are found over the forested areas where the heat flux values are as low as 10 Wm^{-2}. The creeks and ponds also display low heat flux values.

4.4.6 August 22 Surface Evaporative Heat Flux

The values for the evaporative heat flux, shown in Figure 30, range from 430 Wm^{-2} in Clarksville to 630 Wm^{-2} over the forests. A local evaporative heat flux minimum of 510 Wm^{-2} is found over Fort Campbell. The 470 Wm^{-2} isopleth northwest of Fort Campbell corresponds with the runways of the airfield located there. Other low values of E_o are found over Hickory Point (470 Wm^{-2}), Woodlawn (550 Wm^{-2}), and Corbandale (550 Wm^{-2}). The largest values of E_o are found over the forests where values of 630 Wm^{-2} are found. The relatively high values (630 Wm^{-2}) found near the Cumberland power plant occur because the power plant is situated in an open area bordered by trees on three sides and the Cumberland River on the open side. Large E_o values are also found over the numerous creeks, ponds, and croplands.

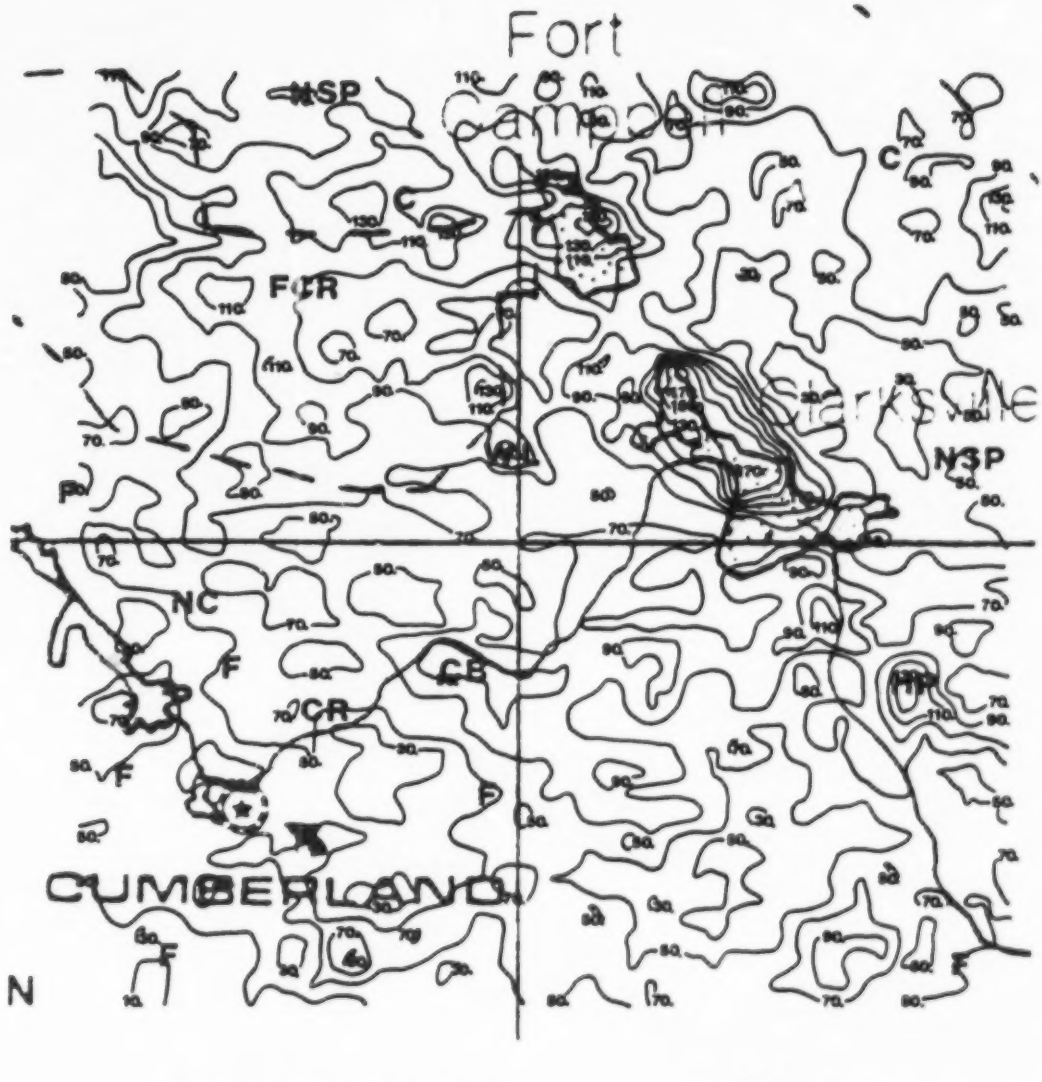

Figure 29. The Clarksville surface heat flux analysis for the early afternoon of 22 August 1978 (Wm^{-2}).

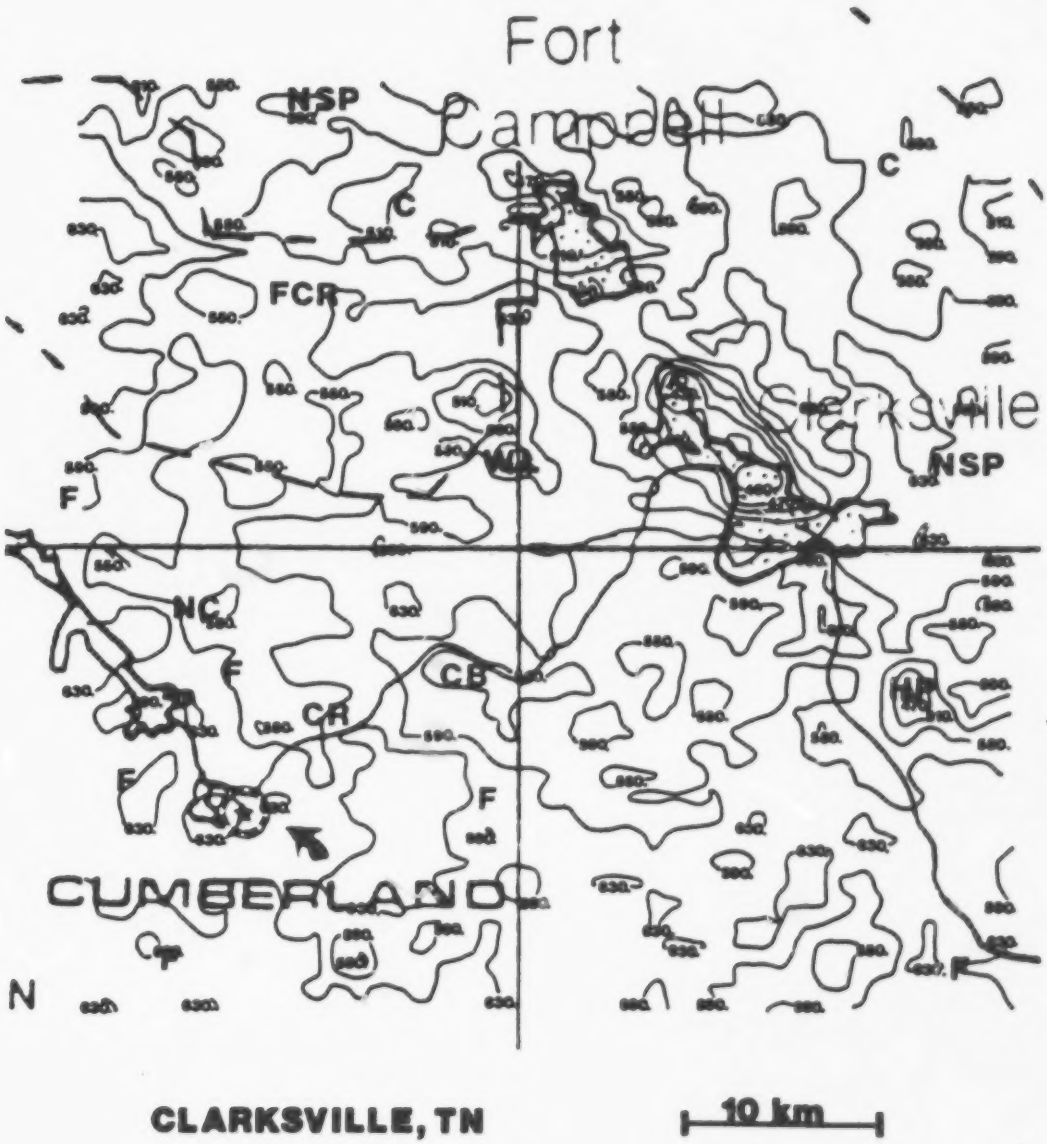

Figure 30. The Clarksville surface evaporative heat flux for the early afternoon of 22 August 1978 (Wm^{-2}).

4.5 Cumberland Albedos

The base map used for the Cumberland albedo study, along with key coded areas, is shown in Figure 31. The flight path for 17 August 1978 of The Pennsylvania State University's airplane is superimposed over the map, and this will be referred to in section 4.6.

Surface albedo values for approximately 1400 LT on 22 August 1978, which were derived from visible satellite measurements, are shown in Figure 32. The surface albedo is defined as the ratio of the reflected solar energy to the incident solar energy at the earth's surface. A simple transfer model for the visible spectrum was used to convert the visible satellite DN values to albedos. The satellite response in the visible range was 0.56 μm to 1.04 μm.

The lowest albedos are found over Kentucky Lake and Lake Barkley where values from 4% to 8% are found. Smoothing of the data removed lower albedo values over these lakes. The forested areas exhibit values from 10% to 14%. The spatial fluctuations of albedos over the forest are due to the variability of the forest density, the woodlot spacing, and the mixing of tree species. The farmlands north of Fort Campbell reveal 14% to 16% albedo values depending on the type of crop being grown. The non-forested Fort Campbell restricted zone (FCR) displays albedo values ranging from 10% to 16%.

These satellite derived albedos agree well with typical albedos for various surfaces which are given by Sellers (1965) and Kung et al. (1964). Kung et al. (1964) found the albedo values of forests to be lower than that of farmlands. The following typical albedos are given by Sellers (1965) for various terrain: deciduous

Figure 31. The base map used for the Cumberland albedo study and the flight path for 17 August 1978 of The Pennsylvania State University's airplane, along with the following key areas coded for easy reference:

LB Lake Barkley

KL Kentucky Lake

CR Cumberland River

CB Corbandale

WL Woodlawn

FCR Fort Campbell Restricted Area

NSP Numerous Small Ponds

NC Numerous Creeks

F Forest and Brushwood

C Cropland and Pasture

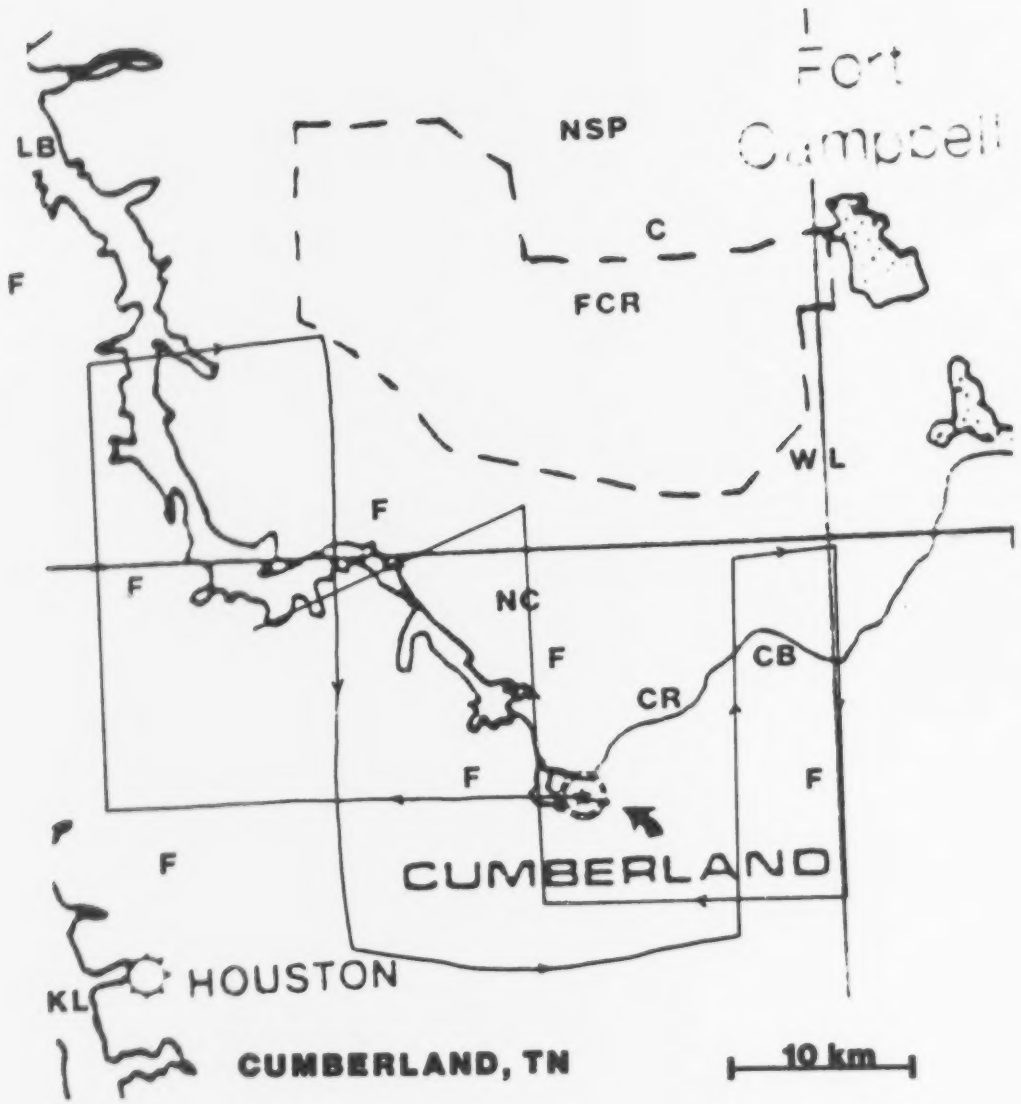
Fort
Campbell
NSP
LB
C
F
FCR
WL
F
F
NC
F
CB
CR
F
F
F
CUMBERLAND
HOUSTON
KL
CUMBERLAND, TN
10 km

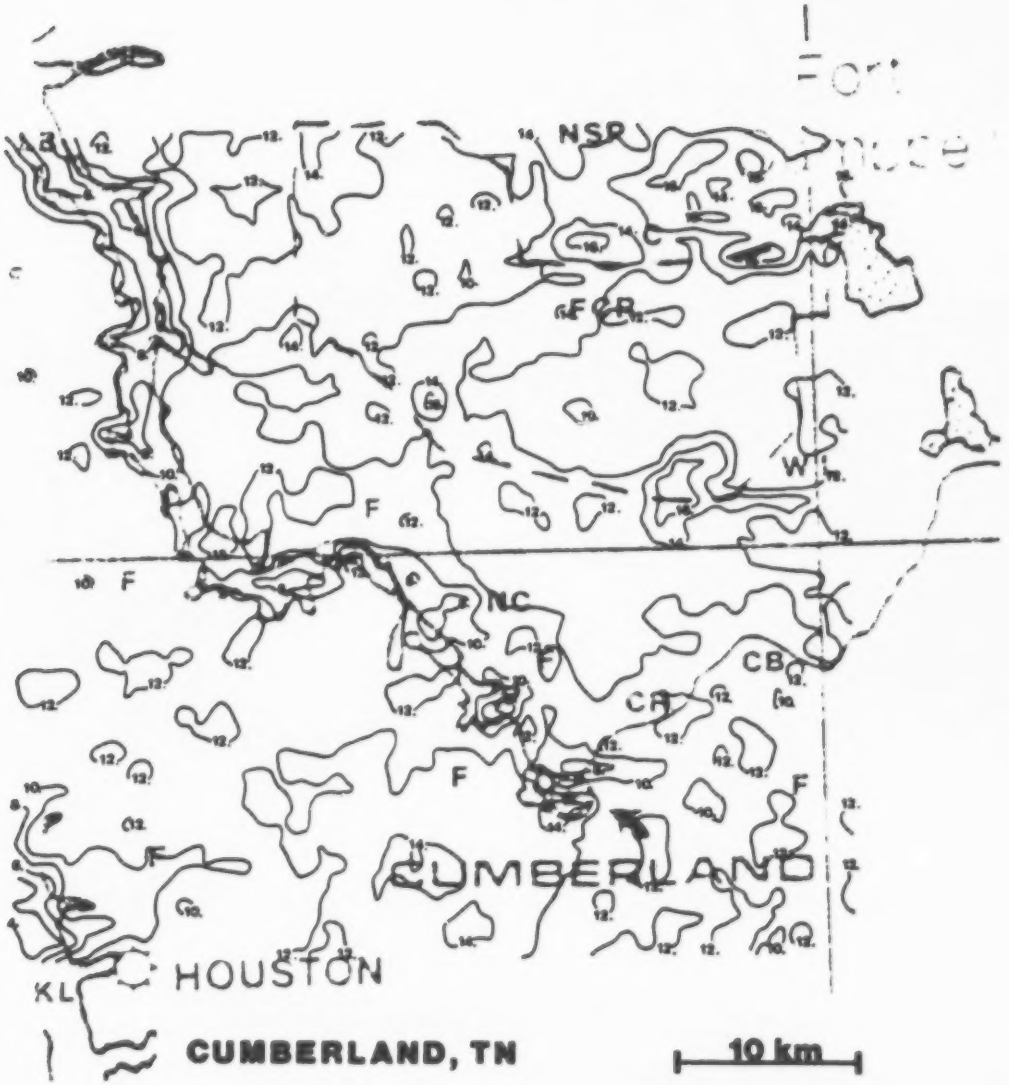

Figure 32. The Cumberland surface albedo analysis (derived from visible satellite measurements) for 1400 LT on 22 August 1978 (%).

forests, 10--20%; coniferous forests, 5--15%; crops, 15--25%; green meadows, 10--20%; black topped roads, 5--10%; dark soil, 5--15%; and water, 3--5% at solar noon.

Kung et al. (1964) observed that the surface albedo is related to the phenological cycle of the vegetation. Lush tree leaves and lower vegetation tend to reflect a greater fraction of incident solar energy than do canopies with sparse tree leaves or vegetation. Soil moisture content may also be a probable factor influencing the surface albedo. Incident rays can enter in all directions when the soil particles and plant surface are covered with a film of water; however, only rays which can reach the surface of the water film within the limiting angle of total reflection can emerge. The surface albedo can also be directly influenced by the soil color and water holding capacity; thus, soil types should be considered when looking at regional surface albedos. However, Kung et al. (1964) believe that the surface albedo difference due to soil types is less important than that due to vegetative covers, at least where bare soils are not common. The surface albedo is also dependent on wavelength. The wavelengths ranging from 0.5 μm to 1.0 μm (near infrared) depend on the solar angle and the viewing angle of the satellite.

4.6 Comparison of Aircraft Measurements with Satellite Derived Albedos, Surface Heat and Evaporative Fluxes

From 10 August to 19 August 1978, The Pennsylvania State University's Aerocommander 680E made nine flights for the STATE project. A detailed description of these flights is given by DiCristofaro and Albrecht (1979). The flight path for one of these

flights is displayed in Figure 31. This flight was a land use study made in the vicinity of the Cumberland power plant. The passes were made at 500 feet (MSL).

Eight radiometers on board the aircraft were used to measure the short and long-wave radiation. The ratio of the reflected short-wave irradiances to the incident irradiances was used to calculate the albedo of the surface. Simpson's Rule (described in the Appendix) was used to calculate the average albedo for each flight pass. The surface albedos derived from the visible satellite measurements, shown in Figure 32, were also averaged for each flight pass through the use of Simpson's Rule.

A comparison of the aircraft and satellite measured albedos for each flight path is given in Table III. The aircraft measured values were 1.5% higher on the average; thus, the agreement was excellent. The largest differences were for pass number three (2.7% difference) and pass number six (2.4% difference). These were the shortest of the nine passes. The best agreement (0.4% difference) was for pass number five which was one of the longest passes. Better results are obtained if a bidirectional transfer model for the visible spectrum is used to convert the visible satellite DN values to albedos.

From 2 August to 28 August 1978, the Boundary Layer Group (BLDG) of the National Oceanic and Atmospheric Administration (NOAA) made airborne turbulence measurements in the vicinity of the Cumberland power plant. Four of the flights (9, 10, 14, and 27 August 1978) were land use studies made at an altitude of approximately 250 to 300 m.

Table III. The Satellite Measured Albedos for 22 August 1978 vs. The Aircraft Measured Albedos for 17 August 1978 at Approximately 1400 LT.

Pass Number	Satellite Albedo (%)	Aircraft Albedo (%)
1	12.4	13.4
2	11.5	13.2
3	11.0	13.7
4	11.8	12.7
5	12.5	12.9
6	11.7	13.1
7	11.3	13.7
8	11.4	13.1
9	11.7	13.4
10	12.1	13.2

A comparison of the aircraft measurements for the four different days with the satellite measurements for 22 August 1978 was made. The aircraft measurements were corrected to surface values by multiplying the aircraft values by $(\frac{h}{h-z_a})$ where h is the height of the mixed layer and z_a is the height of the aircraft. A correction for the time difference was also made. Ching (1980) maintains that it is not valid to neglect synoptic variations; therefore, a comparison of the satellite measurements for 22 August 1978 should not be made with the aircraft measurements for the four different days. Indeed, the largest differences between the aircraft and satellite measurements were for 9, 10, and 14 August 1978. The closest agreement was for 27 August 1978 and these results are

given in Table IV. The filtered aircraft results were obtained from NOAA. The satellite values were obtained from Figures 23 and 24, and Simpson's Rule was used to obtain an average value of H_o and E_o over each flight path. The passes were made over the Land Between the Lakes.

Table IV. The Satellite Measured Heat and Evaporative Fluxes for 22 August 1978 vs. The Aircraft Measurements for 27 August 1978.

Pass Number		Satellite Value (Wm^{-2})	Aircraft Value (Wm^{-2})
2	E_o	498.5	450.5
	H_o	68.0	145.4
3	E_o	527.2	489.7
	H_o	67.0	198.7
5	E_o	533.2	512.0
	H_o	65.2	163.8

The aircraft measured values of the evaporative heat flux were, on the average, 36 Wm^{-2} lower than the satellite measured values. The large heat flux values obtained by the aircraft measurements seem too large and the spatial variation of heat flux is opposite to what is expected. The satellite images shown in Figures 3 through 6 and the daytime surface temperature analysis shown in Figure 19 clearly display lower temperatures over the Land Between the Lakes area; yet, the aircraft measured heat flux values were found to be larger in this region. The aircraft heat

fluxes over the forested areas were approximately the values found for downtown St. Louis (see Figure 14)! Dense vegetation, such as the canopy of trees found in the Land Between the Lakes region, is known to contribute significantly more evaporative than sensible heat flux, i.e. the Bowen ratios are typically small.

4.7 Summary of Results

A large variation of the daytime surface temperature was observed over the Land Between the Lakes and Clarksville areas. Small towns with populations less than 1,000 people exhibited local temperature maxima. The lowest daytime temperatures were observed over the forested areas where a large amount of the evaporation was also observed, thus causing the cooler conditions. The highest daytime temperatures corresponded to the areas of lowest moisture availability and evaporative fluxes, and highest surface heat fluxes. Evaporation is suppressed on dry surfaces which allows a greater partitioning of the net radiation into sensible heat, thus causing greater surface heating. More energy is partitioned into latent heat flux for moist surfaces causing suppressed heating.

The largest diurnal temperature range was found over farmland where the thermal inertia was a minimum. The smallest diurnal temperature variation was found over the bodies of water. Maximum values of thermal inertia were anticipated over the cities of Clarksville and Fort Campbell. This would have reflected the enhanced ability of the urban substrate to store and conduct heat. However, minimum values of thermal inertia were found over some urban areas such as Clarksville and Fort Campbell; thus, no distinct

nighttime temperature maxima were evident. It is evident that warmer nighttime temperatures are also related to higher temperatures during the day not just to P.

The distinct variation of vegetation over the area, or a variation of transpiring surfaces, was responsible for a large change in the heat and evaporative fluxes. Large changes of H_o and E_o were observed over a distance of even a few kilometers. Thus, vegetation is the arbiter of H_o and E_o.

The moisture availability values approached 1.0 over the forested areas which accounts for the large surface evaporative fluxes found there. Shuttleworth and Calder (1979) made evaporation measurements for tall (forest) vegetation for two cases. The comparison was made for conditions when water was freely available on the surface of the vegetation, and for a "potential" condition when there was no significant moisture stress, which is probably an erroneous condition. Moisture availability values of .5 were found for the dry conditions and values of 1.0 were found for the wet conditions. Shuttleworth and Calder (1979) concluded that the status of the surface (i.e., whether it is wet or dry) within a given type of vegetation, is the primary control on the evaporation rate.

The albedo values over the Cumberland area were lowest over the bodies of water and highest over the croplands. The albedos varied by 6% over the various vegetative covers. Agreement between aircraft derived values and those determined from the satellite measurements was close, although there was very little spatial variation in the former.

5.0 INFERRING THE EFFECTS OF SURFACE HEAT FLUX ON PLUME SPREAD AND CONCENTRATION OF CONTAMINANTS

5.1 Atmospheric Dispersion Research

Presently, the most popular method of determining σ_y and σ_z is from the Pasquill-Gifford empirical curves in which σ_y and σ_z are plotted as a function of x. As Panofsky (1969) points out, the main drawback of the Pasquill-Gifford curves is that they do not allow for the effect of terrain roughness. The empirical curves were based on experiments over smooth terrain; therefore, the dispersion over cities and other rough regions is underestimated. The Pasquill-Gifford curves were produced from ground sources and represent averages over a few minutes. Thus, the curves must be adjusted if they are to be used under conditions different from those for which they were constructed.

The classic model used by most atmospheric dispersion scientists for elevated point sources is the Gaussian plume diffusion model. This is described by

$$\chi = \frac{Q}{2\pi\sigma_y\sigma_z\bar{U}} \exp\left(-\frac{y^2}{2\sigma_y^2}\right)\left[\exp\left(-\frac{(z-H)^2}{2\sigma_z^2}\right) + \exp\left(-\frac{(z+H)^2}{2\sigma_z^2}\right)\right] \tag{5}$$

where χ is the ground-level concentration, Q is the source strength, σ_y and σ_z are the standard deviations of the time-averaged plume concentration distribution in the y (cross-wind) and z (vertical)

directions, $\bar{U}$ is the mean horizontal wind, and H is the effective source emission height.

The Gaussian plume model is based on steady-state conditions, homogeneous flow, no atmospheric chemical reactions or gravity fallout, a sampling time of at least ten minutes, and a significant wind speed. Also, for the form of the Gaussian model presented in equation (5), perfect reflection of the plume at the ground is assumed.

Munn et al. (1972) point out that equation (5) does not apply when the winds are light, when serious air quality deterioration can occur. The Gaussian plume dispersion model also assumes that there are no vertical gradients in wind. Also, steady-state homogeneous conditions may be a mathematical convenience rather than reality. The Gaussian plume model does not directly take into account a variable heat flux. In some dispersion studies, such as the one conducted by Venkatram (1980), the surface heat flux was assumed to be 0.3 times the incoming solar radiation. However, it will be shown in section 5.3 that a variable heat flux has an important effect on plume spread and concentration.

Many new methods of estimating dispersion parameters have been suggested in the past few years. One such method was developed by Willis and Deardorff (1974). They studied the turbulence and transfer properties in the laboratory under free convection conditions. Free convection occurs when turbulence is independent of surface drag force such as in the daytime under clear skies and light winds when dispersion is often dominated by convection. The surface heat flux enters the Willis and Deardorff method explicitly;

therefore, this method is used rather than the Pasquill-Gifford method. The Willis and Deardorff method of estimating dispersion parameters is discussed in detail in section 5.2.

5.2 Dispersion from an Elevated Point Source in the Convective Planetary Boundary Layer

Willis and Deardorff (1978) used a laboratory model and Lamb (1978) used a numerical model of the convective planetary boundary layer to study dispersion from an elevated source. The results applied to a continuous point source located within a thermally convecting field in the presence of a simulated uniform mean wind. Free-convection similarity scaling was used to non-dimensionalize the quantities measured. An elevated release height of $z_s = .25\ h$ was chosen by Willis and Deardorff (1978) and $z_s = .26\ h$ was chosen by Lamb (1978), where h is the thickness of the convectively mixed layer.

The simple, workable laboratory model consisted of a deep convective layer heated from below with a capping inversion formed by an overlying stable layer. A detailed description of the model is given by Willis and Deardorff (1974).

The turbulent velocities σ_v and σ_w in the upper part of the planetary boundary layer scale with the convective velocity w_* given by

$$w_* = \left(\frac{gH_o h}{\rho c_p T}\right)^{1/3} , \qquad (6)$$

where H_o is the surface heat flux, ρ is the air density, c_p is the specific heat at constant pressure, and T is the average temperature of the mixed layer. The controlling scales in the mixed layer are w_* and h. This scaling is valid provided the height exceeds L, given by

$$L = -\frac{\rho c_p T}{kgH_o} u_*^3 \quad , \tag{7}$$

where k is the von Karman constant and u_* is the friction velocity.

These scales are then used to nondimensionalize all the variables. The dimensionless time used is

$$t^* = (\frac{w_*}{h})t \quad , \tag{8}$$

where t is the time measured from the centered time of particle release. Taylor's hypothesis, $t \rightarrow \frac{x}{U}$, is used to convert time to a space coordinate, where x is the distance from the pollutant source and U is the simulated uniform mean wind blowing along the x axis. The dimensionless time or distance can then be written as

$$t^* = X = (\frac{w_*}{U})(\frac{x}{h}) \quad . \tag{9}$$

This transformation is valid within the limits of

$$1.2\ w_* \leq U \leq 6\ w_* \quad . \tag{10}$$

Willis and Deardorff (1978) maintain that the lower limit is needed to insure that the mean wind is strong enough so that significant upstream turbulent diffusion does not occur. The upper limit represents the value above which turbulence in the bulk of the mixed layer begins to be significantly affected by shear stress.

The nondimensional mean particle height is defined as

$$\overline{Z} = \int_0^{1.1h} Z\, p_z\, dz \quad , \tag{11}$$

where $p_z\, dz$ is the probability that a particle resides in a horizontal layer between $z - \frac{1}{2}\Delta z$ and $z + \frac{1}{2}\Delta z$. The numerical results of Lamb (1978) are shown in Figure 33 where the nondimensionalized mean height $\overline{Z}$ is plotted as a function of the nondimensionalized downwind distance from the source X. Initially, $\overline{Z}$ remains approximately constant at short distances of X until enough descending particles have been entrained into updraft regions. The Gaussian plume or K-Theory models of turbulent diffusion cannot describe this aspect of diffusion in a convectively mixed layer. $\overline{Z}$ then increases to its equilibrium value of about 0.5 h at X = 1.6, with a slight overshoot of approximately 0.025 h.

The dimensionless vertical and lateral, overall standard deviations of particle displacement are defined, respectively, as

$$(\overline{Z'^2})^{1/2} = \sigma_z = \left[\int_0^{1.1h} (Z-Z_s)^2\, p_z\, dz\right]^{1/2} \tag{12}$$

$$(\overline{Y'^2})^{1/2} = \sigma_y = \left[\int_{-2h}^{2h} Y^2\, p_y\, dy\right]^{1/2} \tag{13}$$

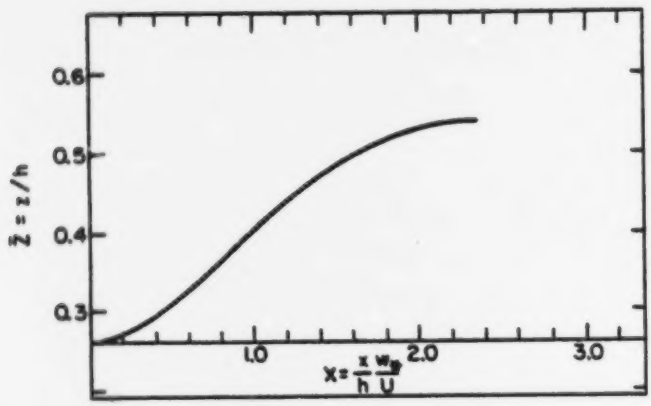

Figure 33. The nondimensional mean particle height ($\bar{Z}$) as a function of the nondimensional downwind distance from the source (X) (from Lamb, 1978).

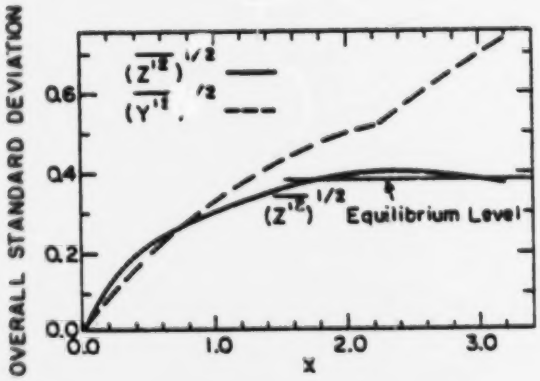

Figure 34. The dimensionless overall standard deviations as a function of the dimensionless downwind distance from the source (from Willis and Deardorff, 1978).

where $p_y\,dy$ is the probability that a particle will appear anywhere in a vertical column between $y - \frac{1}{2}\Delta y$ and $y + \frac{1}{2}\Delta y$. The laboratory results, made by Willis and Deardorff (1978), of the dimensionless overall particle standard deviations are shown in Figure 34 as a function of the dimensionless downstream distance. At the source height, the root-mean-square turbulent vertical velocity, σ_w, is greater than the turbulent lateral velocity component, σ_v; therefore, the vertical spread, σ_z, exceeds the lateral spread, σ_y, at short values of X. The effects of the capping inversion begin to slow the vertical spread by $X \geq 0.8$, until σ_z reaches its equilibrium value of about .38 h with only a slight overshoot. The lateral spread of the plume continually increases with X, with a sharp increase near X = 2.2. Willis and Deardorff (1978) believe this feature is due to some of the particles being trapped for a time in the lateral confines of a large-scale eddy before undergoing accelerated lateral spread once sufficient numbers of particles are carried into an adjacent large-scale eddy.

The dimensionless mean cross-wind integrated concentration is defined as

$$\overline{c}^{y}\,(X,Z) = \frac{\overline{c}^{y}\,(X,Z)\;hU}{Q} \quad , \tag{14}$$

where

$$\overline{c}^{y}\,(X,Z) = \lim_{t\to\infty} \int_{-\infty}^{+\infty} \overline{c}\,(X,Y,Z,t)\;dY \quad . \tag{15}$$

The time dependent point mean concentration is $\overline{c}(X,Y,Z,t)$ and the emission rate is Q. The x, y, and z coordinates nondimensionalized by h are represented by X, Y, and Z in equations (14) and (15). The numerical simulation of $\overline{C}^y$ performed by Lamb (1978) is shown in Figure 35. This is for an elevated source height of $z_s = 0.26$ h and a time average over a period of about 20 minutes or longer. The centerline of the plume descends from the source to a point near $x \sim \frac{0.6hU}{w_*}$, where the centerline intercepts the ground, until a distance $x \sim \frac{1.2hU}{w_*}$. The plume then begins to ascend again.

Willis and Deardorff (1976) computed the cross-wind integrated concentrations for a source height of $z_s = 0.067$ h. After comparing the results of the lower release height with the results computed for $z_s = 0.25$ h, they concluded that the source height is a dominant influence until the concentration maximum first reaches the ground. Beyond that distance, the concentration fields are very similar.

The ground-level values of the mean cross-wind integrated concentration, $\overline{C}^y(X,0)$, as computed by the numerical study made by Lamb (1978), are presented in Figure 36. Comparing these results with the Gaussian plume results, Lamb (1978) found the ground-level concentrations to be larger than those predicted by the Gaussian plume formula at all distances from the source.

5.3 St. Louis and Cumberland Plume Characteristics

The heat flux maps for St. Louis, the Land Between the Lakes, and Clarksville shown in Figures 14, 23, and 29 display a large variation of heat flux over a distance of a few kilometers. The

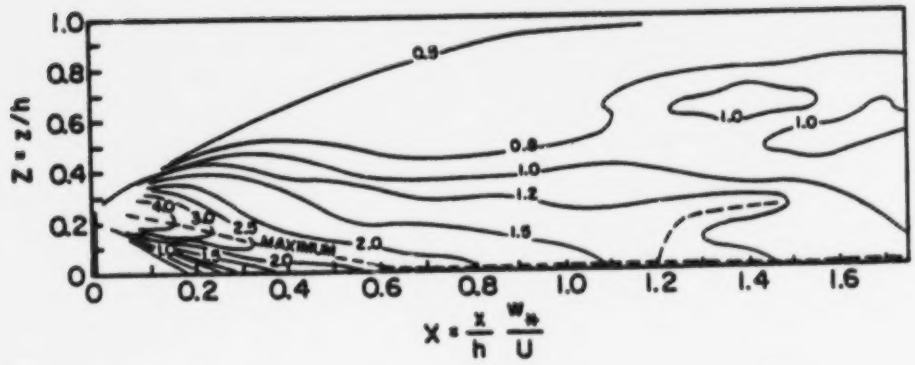

Figure 35. The dimensionless mean cross-wind integrated concentration ($\overline{C}^y$) for an elevated source height of z_s=0.26h indicated by the vertical bar. The centerline of the plume is represented by the dashed line (from Lamb, 1978).

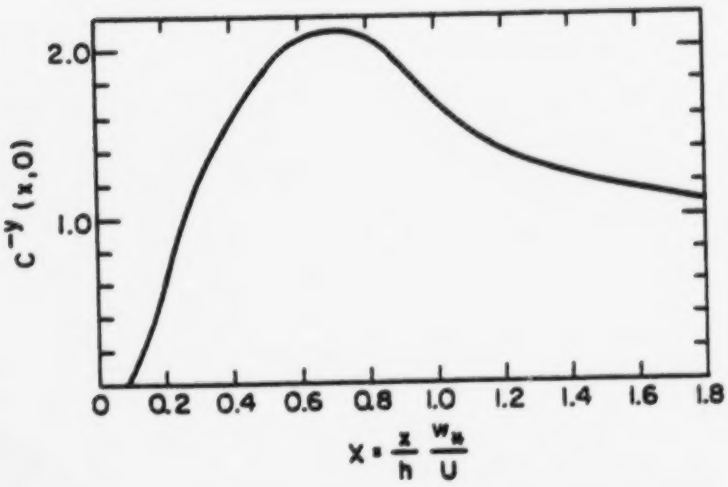

Figure 36. The ground-level values of the mean cross-wind integrated concentration ($\overline{C}^y(x,0)$) from a continuous point source of height z_s=0.26h as a function of the dimensionless downwind distance from the source (from Lamb, 1978).

purpose of this study is to investigate the impact of this variable heat flux on the plume spread and concentration.

Typical values for the height of the mixed layer (h), wind speed (U), mean temperature of the layer ($\overline{T}$), density (ρ), and specific heat (c_p) used to compute w_* and X are listed in Table V. The effect of a variable heat flux on plume spread and concentration is studied at a distance of 1 km and 2 km from the source. The results for x = 1 km are given in Table VI and the results for x = 2 km are given in Table VII. The values of heat flux listed in Tables VI and VII are representative values found over St. Louis and Cumberland during the period studied.

Table V. The Values Used to Compute w_* and X.

$h = 1000$ m

$U = 2$ msec^{-1}

$\rho = 1.2$ kgm^{-3}

$\overline{T} = 299°K$

$c_p = 1004$ Jkg^{-1} K^{-1}

The following discussion is in reference to the results presented in Tables VI and VII. These results were obtained by the method described in section 5.2.

The nondimensional mean particle height ($\overline{Z}$), at x = 1 km, increases from .28 for $H_o = 10$ Wm^{-2} to .38 for $H_o = 200$ Wm^{-2}. The mean particle height, at x = 2 km, increases from .34 for $H_o = 10$ Wm^{-2} to .51 at $H_o = 200$ Wm^{-2}.

Table VI. The Effect of Surface Heat Flux on Various Plume Spread and Concentration Parameters at a Distance of 1 km from the Source.

$H_o(Wm^{-2})$	w_*	X	$\bar{z}$	σ_z	σ_y	$\bar{c}^y$	$\bar{c}^y(x,0)$	x_g(m)	$\bar{\chi}(x,0,0)$
10	.65	.32	.28	.18	.13	1.9	1.3	1846	3.99
50	1.12	.56	.32	.23	.20	1.2	1.9	1071	3.79
100	1.41	.70	.34	.25	.25	1.0	2.1	851	3.35
200	1.77	.88	.38	.28	.29	0.9	1.9	678	2.61

Table VII. The Effect of Surface Heat Flux on Various Plume Spread and Concentration Parameters at a Distance of 2 km from the Source.

H_o (Wm^{-2})	w_*	X	$\bar{z}$	σ_z	σ_y	$\bar{c}^y$	$\bar{c}^y(x,0)$	x_g (m)	$\bar{\chi}(x,0,0)$
10	.65	.65	.34	.25	.24	1.0	2.1	1846	3.49
50	1.12	1.12	.42	.31	.36	.95	1.5	1071	1.66
100	1.41	1.41	.48	.35	.43	.95	1.2	851	1.11
200	1.77	1.77	.51	.38	.48	1.0	1.1	678	.91

The dimensionless vertical $((\overline{z'^2})^{1/2}$ or σ_z) and lateral $((\overline{y'^2})^{1/2}$ or σ_y), overall standard deviations of particle displacement also increase with increased heat flux. Under low heat flux conditions and at short values of X, σ_z exceeds σ_y at both x = 1 km and x = 2 km. At x = 1 km, σ_z equals σ_y at H_o = 100 Wm^{-2}. The capping inversion then begins to slow the vertical spread of the plume so that σ_y exceeds σ_z at H_o = 200 Wm^{-2} and x = 1 km. At x = 2 km, σ_y exceeds σ_z at H_o = 50 Wm^{-2}.

The nondimensionalized mean cross-wind integrated concentration ($\overline{C}^y$) peaks at 1.9 for H_o = 10 Wm^{-2}. $\overline{C}^y$ decreases to 0.9 under the largest heat flux conditions (200 Wm^{-2}). At x = 2 km, $\overline{C}^y$ varies from 1.0 to .95 with no discernable pattern.

The ground-level value of the mean cross-wind integrated concentration ($\overline{C}^y(x,0)$), at x = 1 km, peaks at 2.1. This corresponds with a 100 Wm^{-2} heat flux. At x = 2 km, $\overline{C}^y(x,0)$ peaks at a lower heat flux (10 Wm^{-2}). The lowest ground-level values, at x = 2 km, are found with the highest heat fluxes.

Lamb (1978) found that the maximum ground-level cross-wind integrated concentrations occurred at

$$x_g = \frac{0.6hU}{w_*} \quad . \tag{16}$$

Using this equation, the maximum value of x_g (1846 m) was found under the lowest heat flux conditions (10 Wm^{-2}). Similarly, the minimum value of x_g (678 m) was found under the highest heat flux conditions (200 Wm^{-2}).

The mean cross-wind integrated concentrations were used to compute the mean ground-level point concentrations by the following method. The mean cross-wind integrated concentration is defined as

$$CIC = \int_{-\infty}^{+\infty} \chi \, dy = \frac{Q}{U} F(z) \quad , \tag{17}$$

where χ is the point concentration, Q is the emission rate, and F(z) is a dispersion function which describes the growth of the plume in the z direction. The point concentration is defined as

$$\chi = \frac{Q}{U} G(y) \, F(z) \quad , \tag{18}$$

where G(y) is a dispersion function which describes the growth of the plume in the y direction. Since the cross-wind integrated concentration is already known, then one only needs to know G(y) to compute the point concentration. G(y) is defined as

$$G(y) = \frac{1}{\sqrt{2\pi}\,\sigma_y} \exp\left(-\frac{y^2}{2\sigma_y^2}\right) \quad , \tag{19}$$

which reduces to

$$G(y) = \frac{1}{\sqrt{2\pi}\,\sigma_y} \tag{20}$$

for centerline plume concentrations or at y = 0. The mean ground level point concentration is then

$$\overline{\chi}(x,0,0) = \frac{CIC}{\sqrt{2\pi}\,\sigma_y} \quad . \tag{21}$$

Lamb (1978) expressed the mean point concentration in terms of Q/hU; however, this is a constant factor in this study. It is believed that although the heat flux changes dramatically over a distance of a few kilometers, the height of the mixed layer is dependent on the overall integrated heat flux, so h can remain constant (Panofsky, 1980).

At x = 1 km, $\overline{\chi}(x,0,0)$ decreases from 3.91 at H_o = 10 Wm^{-2} to 2.61 at H_o = 200 Wm^{-2}. At x = 2 km, $\overline{\chi}(x,0,0)$ decreases from 3.49 at H_o = 10 Wm^{-2} to .91 at H_o = 200 Wm^{-2}.

Figure 37 displays the mean ground-level point concentration as a function of the distance from the source for three constant heat flux values. As the heat flux increases, the closer the point of maximum ground concentration is to the source. The maximum ground-level point concentration is apparently independent of the heat flux and occurs at 4.1; thus, χ_{max} can be expressed as

$$\chi_{max} = 4.1\ (\frac{Q}{hU}) \quad . \tag{22}$$

The inverse heat flux plotted as a function of the distance from the source of the maximum point concentration (x_{max}) is shown in Figure 38. As $H_o \to \infty$, $(H_o)^{-1} \to 0$ and $x_{max} \to 0$. Likewise, the smaller the heat flux, the farther the maximum ground-level point concentration is from the source.

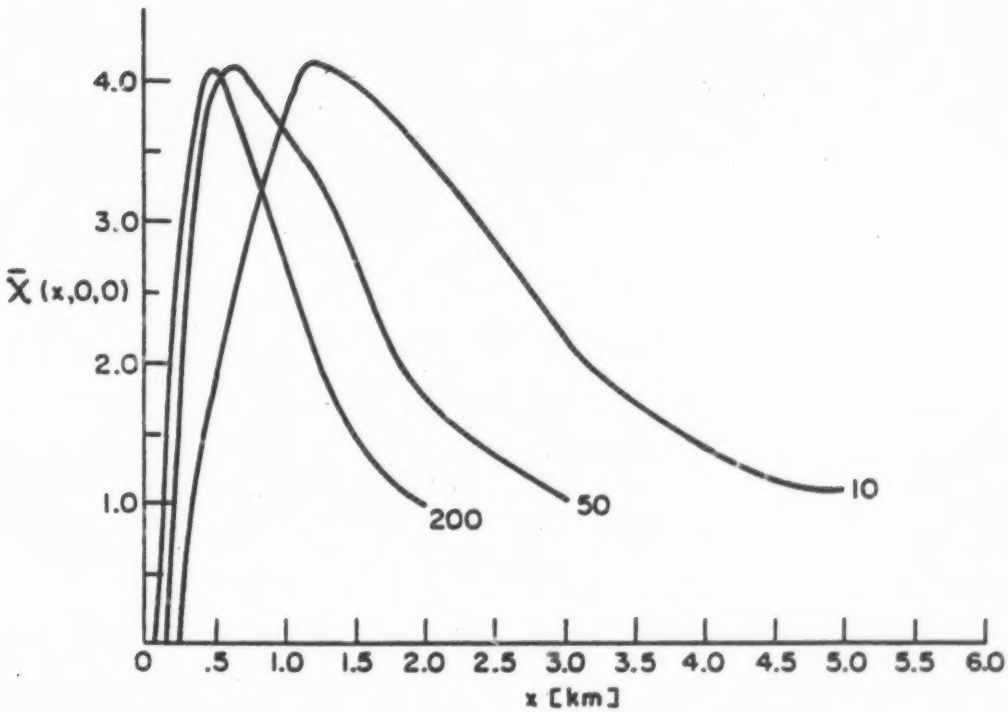

Figure 37. The mean ground-level point concentration ($\bar{\chi}(x,0,0)$) as a function of the downstream distance from the source for H_o=200, 50, and 10 Wm^{-2}.

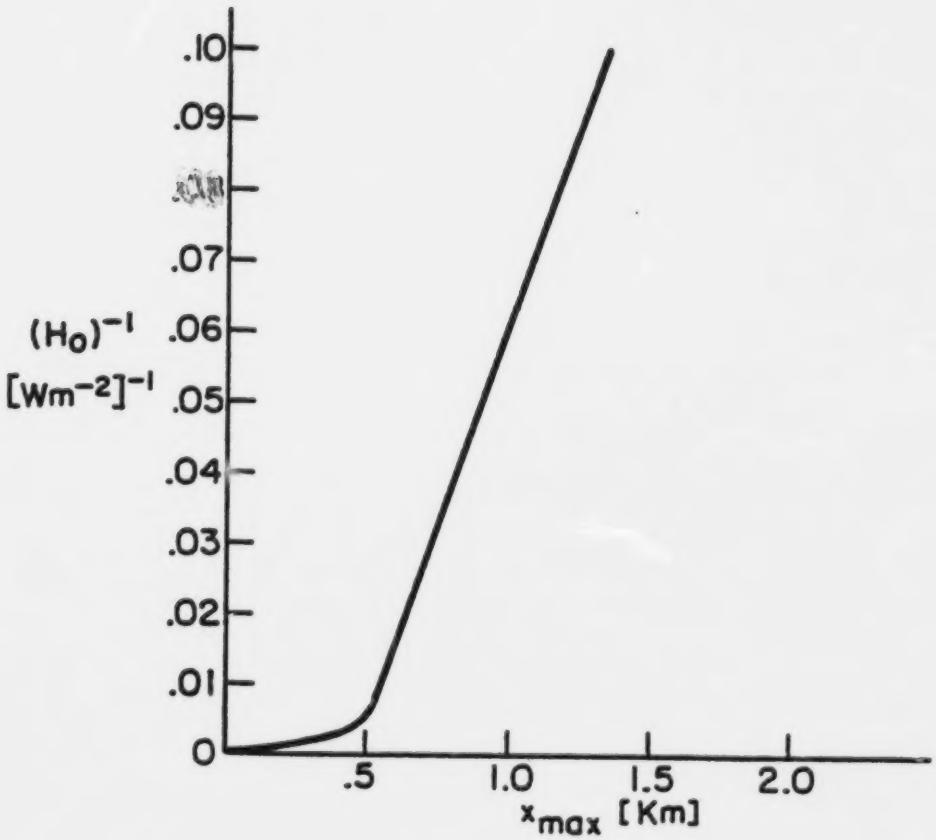

Figure 38. The inverse heat flux $(H_o)^{-1}$ as a function of the distance from the source of maximum point concentration (x_{max}).

5.4 Summary of Results

The Willis and Deardorff method of free convection scaling was used to infer the effects of surface heat flux on plume spread and concentration.

An increased heat flux (H_o) causes an increased convective vertical velocity (w_*) which was found to cause an increase of the nondimensional mean particle height ($\bar{z}$). The largest increases occurred 2 km from the source where the particles have had a longer time to rise.

The increased vertical velocity caused by the increased surface heat flux, also caused an increase of the vertical spread (σ_z) of the plume. An increased heat flux was also found to cause an increase of the lateral spread (σ_y) of the plume. The largest values of σ_y and σ_z were found at x = 2 km under the largest heat flux conditions (200 Wm^{-2}).

The largest mean cross-wind integrated concentrations ($\overline{C}^y$) were found under the lowest heat flux conditions (10 Wm^{-2}) where there was the least amount of vertical mixing of the plume. The largest variation of $\overline{C}^y$ was found at x = 1 km. Farther from the source, at x = 2 km, the heat flux was not an important consideration.

At x = 1 km, the largest ground-level values of the mean cross-wind integrated concentration ($\overline{C}^y(x,0)$) were found at H_o = 100 Wm^{-2}. Farther from the source, at x = 2 km, the largest concentrations were found under the lowest heat flux conditions (10 Wm^{-2}).

The smaller vertical velocities associated with lower heat fluxes caused the location of the maximum ground concentration (x_g)

to be farthest from the source. The pollutant was brought down closer to the source under higher heat flux conditions. A difference in x_g of over 1 km was found for heat fluxes that varied from 10 Wm^{-2} to 200 Wm^{-2}.

The ground-level point concentrations ($\bar{\chi}(x,0,0)$) were largest for smallest heat fluxes due to less vertical mixing. At x = 2 km, a very large difference of $\bar{\chi}$ was found between H_o = 10 Wm^{-2} and 200 Wm^{-2}.

The maximum ground-level point concentrations (χ_{max}) were found to be independent of heat flux, but not independent of the distance from the source. As the heat flux increased, the vertical spread of the plume increased so that the point of maximum concentration was found closer to the source. For an infinitely large heat flux, χ_{max} would be found at the source.

It has been shown in preceding chapters that heat flux varies substantially over different terrain. This chapter has proved that this variable heat flux has an important effect on plume spread and concentration. This variable heat flux should be an important consideration when one models dispersion from a power plant. The variable heat flux should also be considered when one plans to build a power plant. Large surface heat fluxes (200 Wm^{-2}) are found over urban and industrial centers; whereas, low surface heat fluxes (50 Wm^{-2}) are found over forested areas. The higher the heat flux, the closer the maximum ground concentrations are to the source. It is therefore important to consider the land use in the downwind direction of a power plant.

6.0 CONCLUSIONS

A method has been presented that couples a boundary layer model with satellite derived surface temperatures to deduce values of moisture availability, thermal inertia, heat and evaporative fluxes. A sophisticated satellite image display system was used to determine these various parameters from remotely sensed data. This system saved a tremendous amount of time compared to earlier methods of data processing, and increased the accuracy of the final product.

For the three cases studied, the maximum daytime surface temperatures corresponded to the minimum values of moisture availability and this was found in the urban centers. The maximum nighttime surface temperatures were found to be related to the maximum thermal inertia values and this was found over the bodies of water and the urban center of St. Louis. Clarksville and Fort Campbell displayed minimum values of P; therefore, no distinct nighttime temperature maxima were observed. Thus, it was seen that M and P were very much responsible for the formation of important temperature variations over the urban-rural complex. The warmer nighttime temperatures were also related to higher temperatures during the day.

Direct measurements of heat and evaporative fluxes are very costly and quite cumbersome. A reliable method of measuring H_o and E_o remotely without the need for surface or aircraft instrumentation has been presented. Maxima of H_o and minima of E_o were located

in the urban centers and these regions corresponded closely to the sites of maximum daytime temperatures. The opposite held true for the rural areas. Small Bowen ratios were found over vegetated areas and Bowen ratios of approximately 1.0 were found over the urban centers. Hence, a large fraction of the land use variability in heat and evaporative fluxes is caused by variability in rates of evapotranspiration.

Satellite determined measurements of heat and evaporative fluxes and visible channel albedos were compared to corresponding values made by aircraft. In the case of surface heat flux the agreement was poor; with surface evaporative flux there was some agreement, while the albedos compared very closely.

Heat flux values are an important input to mesoscale and diffusion models; however, their values are often surmised. The Willis and Deardorff method of estimating dispersion parameters was used to infer the effects of surface heat flux on plume spread and concentration. Most importantly, it was shown that the ground-level point concentrations were largest for the smallest heat fluxes; however, the maximum ground-level point concentrations were found to be independent of heat flux. χ_{max} was not independent of the distance from the source, though. This variable heat flux effect on plume spread and concentration should be an important input to diffusion models. This should also be an important consideration in choosing the sites of future power plants.

Further research is needed to verify the satellite determined surface heat fluxes with simultaneous direct measurements. Also, a

comparison of the dispersion parameters derived by the Willis and Deardorff method with real diffusion experiments is needed when the surface heat flux is known.

APPENDIX

DESCRIPTION OF SIMPSON'S RULE

The satellite derived and aircraft measured albedos listed in Table III and the satellite derived heat and evaporative flux values listed in Table IV were calculated using Simpson's Rule. This can be expressed as:

$$\int_{x_o}^{x_n} f(x)dx \cong \frac{\ell}{3} (f_o + 4f_1 + 2f_2 + 4f_3 + 2f_4 + \ldots + 2f_{n-2} + 4f_{n-1} + f_n) \quad ,$$

where: $\ell = \frac{x_n - x_o}{n}$, $x_n > x_o$

n = number of subintervals = 2, 4, 6, 8, ...

This is presented graphically in Figure 39.

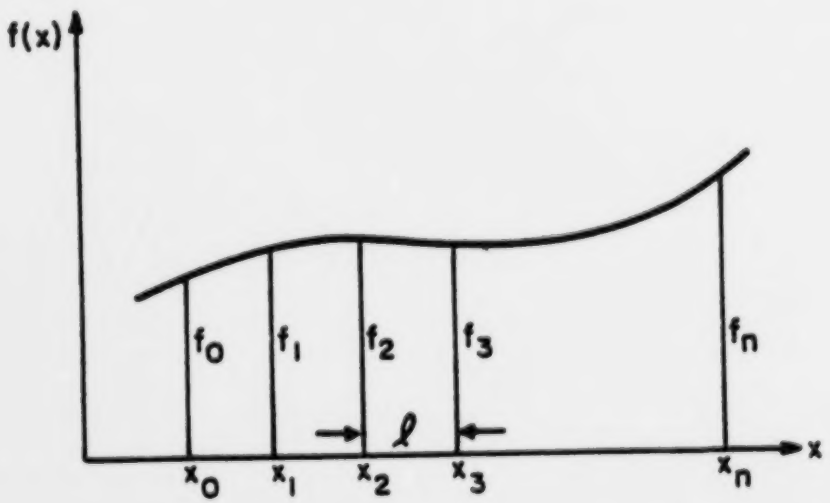

Figure 39. Graphic representation of Simpson's Rule.

REFERENCES

Augustine, J. A., 1978: A Detailed Analysis of Urban Ground Temperature and Albedo Using High-Resolution Satellite Measurements. M.S. Thesis, Department of Meteorology, The Pennsylvania State University.

Blackadar, A. K., 1979: High resolution models of the planetary boundary layer. Advances in Environmental Science and Engineering, Vol. I, Pfafflin and Ziegler, Ed. New York, Gordon and Breach, 50-85.

Boland, F. E., 1977: A Model for Determining Surface Temperatures and Sensible Heat Fluxes Over the Urban-Rural Complex. M.S. Thesis, Department of Meteorology, The Pennsylvania State University.

Braham, R. E. and Wilson, D., 1978: Effects of St. Louis on convective cloud heights. J. Appl. Meteor., 17, 587-592.

Budyko, M. I., 1963: Evaporation Under Natural Conditions. Jerusalem, Sivan Press, 130 pp.

Carlson, T. N., Augustine, J. A., and Boland, F. E., 1977: Potential application of satellite temperature measurements in the analysis of land use over urban areas. Bull. Amer. Meteor. Soc., 58, 1301-1303.

Carlson, T. N. and Boland, F. E., 1978: Analysis of urban-rural canopy using a surface heat flux/temperature model. J. Appl. Meteor., 17, 998-1013.

Carlson, T. N., Dodd, J. K., Benjamin, S. G., and Cooper, J. N., 1980: Satellite estimation of the surface energy balance, moisture availability and thermal inertia. (to be published).

Chandler, T. J., 1965: The Climate of London. London, Hutchinson and Co., 292 pp.

Changnon, S. A., 1978: Urban effects on severe local storms at St. Louis. J. Appl. Meteor., 17, 578-586.

Ching, J. K., 1980: Private communication.

Ching, J. K., Clarke, J. F., and Godowitch, J. M., 1978: Variability of the heat flux and mixed layer depth over St. Louis, Missouri. WMO Tech. Note No. 510, 71-78.

REFERENCES (Continued)

Cogan, J. L. and Willand, J. H., 1974: Mapping the sea surface temperature by the NOAA-2 satellite. Prepared for the Environmental Prediction Research Facility, Naval Postgraduate School, Monterey, California 93940, by Environmental Research and Technology, Inc., 72 pp.

DiCristofaro, D. C. and Albrecht, B. A., 1979: Flight descriptions and data reduction procedures for the Pennsylvania State University aircraft measurements during STATE. Prepared for the Environmental Protection Agency, Washington, D. C., 90 pp.

Dodd, J. K., 1979: Determination of Surface Characteristics and Energy Budget Over an Urban-Rural Area Using Satellite Data and a Boundary Layer Model. M.S. Thesis, Department of Meteorology, The Pennsylvania State University.

Duckworth, F. S. and Sandberg, J. S., 1954: The effect of cities upon horizontal and vertical temperature gradients. Bull. Amer. Meteor. Soc., 35, 198-207.

Hicks, B. B., Hyson, P., and Moore, C. J., 1975: A study of eddy fluxes over a forest. J. Appl. Meteor., 14, 58-66.

Idso, S. B., Jackson, R. D., and Reginato, R. J., 1976: Compensating for environmental variability in the thermal inertia approach to remote sensing of soil moisture. J. Appl. Meteor., 15, 811-817.

Kocin, P. J., 1979: Remote Estimation of Surface Moisture Over a Watershed. M.S. Thesis, Department of Meteorology, The Pennsylvania State University.

Kung, E. C., Bryson, R. A., and Lenschow, D. H., 1964: Study of a continental surface albedo on the basis of flight measurements and structure of the earth's surface cover over North America. Mon. Wea. Rev., 12, 543-564.

Lamb, R. G., 1978: A numerical simulation of dispersion from an elevated point source in the convective boundary layer. Atmos. Env., 12, 1297-1304.

Landsberg, H. E., 1979: The effects of man's activities on climate. Food, Climate and Man, M. R. Biswas, Ed., New York, John Wiley and Sons, Inc., 187-236.

REFERENCES (Continued)

Matson, M., McClain, E. P., McGinnis, D. F., and Pritchard, J. A., 1978: Satellite detection of urban heat islands. Mon. Wea. Rev., 106, 1725-1734.

Mitchell, J. M., 1961: The temperature of cities. Weatherwise, 14, 224-229.

Munn, R. E., Eggleton, A. E., Facy, L., Pack, D. H., and Schmidt, F. H., 1972: Dispersion and forecasting of air pollution. WMO Tech. Note No. 121, 116 pp.

Nappo, C. J., 1975: Parameterization of surface moisture and evaporation in a planetary boundary layer model. J. Appl. Meteor., 14, 289-296.

Nkemdirim, L. C., 1976: Dynamics of an urban temperature field--a case study. J. Appl. Meteor., 15, 818-828.

Oke, T. R., 1978: Boundary Layer Climates. London, Methuen and Co. LTD, 372 pp.

Oke, T. R., 1979a: Review of Urban Climatology 1973-1976. WMO Tech. Note No. 169.

Oke, T. R., 1979b: Advectively-assisted evapotranspiration from irrigated urban vegetation. Bound. Layer Meteor., 17, 167-173.

Panofsky, H. A., 1969: Air pollution meteorology. American Scientist, 57, 269-285.

Panofsky, H. A., 1980: Private communication.

Price, J. C., 1979: Assessment of the urban heat island effect through the use of satellite data. Mon. Wea. Rev., 107, 1554-1557.

Reginato, R. J., Idso, S. B., Vedder, J. F., Jackson, R. D., Blanchard, M. B., and Goettelman, R., 1976: Soil water content and evaporation determined by thermal parameters obtained from ground-based and remote measurements. J. Geophys. Res., 81, 1617-1620.

Schiermeier, F. A., Wilson, W. E., Pooler, F., Ching, J. K., and Clarke, J. F., 1979: Sulfur transport and transformation in the environment (STATE): a major EPA research program. Bull. Amer. Meteor. Soc., 60, 1303-1312.

Sellers, W. D., 1965: Physical Climatology. Chicago, The University of Chicago Press, 272 pp.

REFERENCES (Continued)

Shuttleworth, W. J. and Calder, I. R., 1979: Has the Priestly-Taylor equation any relevance to forest evapotranspiration? J. Appl. Meteor., 5, 639-646.

Spittlehouse, D. L. and Black, T. A., 1979: Determination of forest evapotranspiration using bowen ratio and eddy correlation measurements. J. Appl. Meteor., 5, 647-653.

Tanner, C. B. and Pelton, W. G., 1960: Potential evapotranspiration estimates by the approximate energy balance method of Penman. J. Geophys. Res., 65, 3391-3412.

Tennekes, H., 1973: A model for the dynamics of the inversion above a convective boundary layer. J. Atmos. Sci., 30, 558-567.

Venkatram, A., 1980: Dispersion from an elevated source in a convective boundary layer. Atmos. Env., 14, 1-10.

White, J. M., Eaton, F. D., and Auer, A. H., 1978: The net radiation budget of the St. Louis metropolitan area. J. Appl. Meteor., 17, 593-599.

Willis, G. E. and Deardorff, J. W., 1974: A laboratory model of the unstable planetary boundary layer. J. Atmos. Sci., 31, 1297-1307.

Willis, G. E. and Deardorff, J. W., 1976: A laboratory model of diffusion into the convective planetary boundary layer. Quart. J. Roy. Meteor. Soc., 102, 427-445.

Willis, G. E. and Deardorff, J. W., 1978: A laboratory study of dispersion from an elevated source within a modeled convective planetary boundary layer. Atmos. Env., 12, 1305-1311.